Control of friction on the atomic scale

INAUGURALDISSERTATION

zur Erlangung der würde eines Doktors der Philosophie
vorgelegt der
Philosophisch - Naturwissenschaftlichen Fakultät der
Universität Basel

von

Anisoara Socoliuc
aus Rumänien

Institut für Physik
Universität Basel

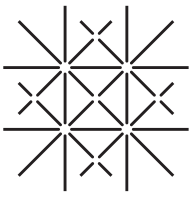

Basel, 2005

Vorgelegt der Philosophisch-Naturwissenschaftlichen Fakultät auf Antrag der Herren Professoren:

Prof. Dr. E. Meyer
Prof. Dr. H.-J. Güntherodt

Basel, den 24 Mai 2005

Prof. Dr. H.-J. Wirz, Dekan

Abstract

"*The modern world depends upon the smooth and satisfactory operation of countless tribological systems.*" B.N.J. Persson

Measuring and controlling friction on the atomic scale is the main goal of this thesis. Nowadays, fundamental studies of friction on nanometer-scale are mandatory, since frictional forces become more and more relevant as the scale of nanoelectromechanical devices is reduced. Despite the increased ratio between surface and volume forces in these devices, we will show how an appropriate design and manipulation of the sliding components can result in smooth motion with minimum energy consumption. All our frictional studies are performed by means of a home-built Atomic Force Microscope (AFM) under ultra high vacuum (UHV) and room temperature conditions. The preparation of samples under UHV conditions allowed the study of clean surfaces, free of water or adsorbates. Friction experiments were thence conducted on dry and clean surfaces, without lubricants. Typical friction signals obtained in AFM measurements present stick-slip characteristics, when the tip moves over the atomic corrugated surface. The jump of the tip from one energy minimum to another is accompanied by instabilities essential for dissipation. Chapter 3 shows that by decreasing the normal force a transition from atomic stick-slip to continuous sliding is observed and a new regime of ultra-low friction is encountered. The transition is described in the framework of the classical Tomlinson model introducing a parameter η, which compares the strength of the lateral atomic surface potential to the stiffness of the contact under study. For $\eta \gg 1$ a dissipative regime of sliding is encountered, whereas for $\eta \leq 1$ sliding occurs with negligible dissipation. This parameter can be tuned experimentally by varying the normal load on the contact. Chapter 4 presents an alternative method based on induced perturbations under resonance condition, which lead to a reduction of friction to negligible values in a controlled way. The regime of zero friction is achieved by applying a periodic excitation between tip and sample at frequencies corresponding to the normal modes of the combined tip-surface system. This method was verified on different surfaces, ionic crystals and mica.

An opposite effect on the nanoscale is wear. Under wear the surfaces involved in the contact experience irreversible changes. In order to understand the conditions under which this process is initiated, and how it develops, we studied the wear process between the AFM tip and insulating and metallic surfaces. Chapter 5 presents a detailed study of the formation of regular topographic structures on a KBr surface under repeated scanning. After the removal of single atomic layers has started, the debris is moved and reorganized due to the interplay between friction-induced strain and erosion, transport of material by the action of the tip, and possibly diffusion. 1D and 2D ripple structures are thus developed.

All these results contribute to a better understanding and control of funda-

mental friction problems which may help to improve the functioning of nanoscale devices.

Contents

Chapter 1

Introduction in Nanotribology

1.1 Motivation for studying frictional properties at atomic scale

"*Sliding friction is not just a nuisance. Without friction there will be no violin music and it would be impossible to walk...*"

In this way B.N.J. Persson starts his book "Sliding Friction. Physical Principles and Application" about one of the oldest phenomena, which is essential for daily life [1]. He insists on the necessity of a better understanding of many aspects of sliding friction, which is important for the progress of technology. Magnetic storage, recording systems, motors, aerospace components are just few examples, whose functioning is strongly related to our capability of producing durable low-friction surfaces and lubricant fluids. There are cases in which an opposite effect is desired, for instance, increased friction between the tyres of a car and the road during braking.

Friction has been studied for several centuries and remarkable scientists established macroscopic friction laws valid up to now. Leonardo da Vinci can be named the father of modern tribology (Greek tribos: rubbing). He studied an

incredible manifold of tribological subtopics such as: friction, wear, bearing materials, plain bearings, lubrication systems, gears, screw-jacks, and rolling-element bearings. 150 years before "Amontons" Laws of Friction were introduced, he had already recorded them in his manuscripts [2, 3]. To the pioneers in tribology one counts besides Leonardo da Vinci also Guillaume Amontons [4], John Theophilius Desanguliers , Leonard Euler [5, 6], and Charles-Augustin Coulomb [7]. These pioneers brought tribology to a standard, and their findings still apply to many engineering problems today. We can summarize them in the following three laws:

1.The force of friction is directly proportional to the applied load. (1^{st} da Vinci-Amontons Law).

2.The force of friction is independent of the apparent area of contact. (1^{st} da Vinci-Amontons Law).

3.Kinetic friction is independent of the sliding velocity. (Coulomb's Law).

These three laws were attributed to dry friction only, as it has been well known since ancient times that lubrication modifies the tribological properties significantly. Around 1880, Reynolds recognized the hydrodynamic nature of lubrication, and introduced a theory of fluid-film lubrication. Still today, Reynolds' steady state equation of fluid film lubrication is valid for hydrodynamic lubrication of thick films. In the twentieth century both dry friction and lubricated friction theories were further developed. The adhesion concept of friction, already proposed by Desanguliers, was applied with great success by Bowden and Tabor to metal-metal interfaces [8]. Adhesion was related to the force required to separate two bodies in contact. In their model the concept of the *real contact area* was introduced. The real area of contact is made up of a large number of small regions of contact, in the literature called *asperities* or junctions of contact, where atom-to-atom contact takes place, see Fig. 1.1. In dry sliding contacts between flat surfaces friction can be modelled as elastic and plastic deformation forces of the asperities in contact [8, 9]. Bowden and Tabor assumed that friction is proportional to both the real contact area and a mean lateral force per unit area, the so-called shear strength:

$$F_F = \sigma A_R = \frac{\sigma}{p_m^*} F_N, \tag{1.1}$$

where A_R is the real area of contact and σ is the shear strength. They considered purely plastic deformation of the asperities until the contact area of each junction has grown large enough to carry its part of the normal load. The contact area can be rewritten as $A_R = F_N/p_m^*$, where p_m^* is the yield pressure of the asperity, which is significantly smaller than the yield pressure of the bulk material due to its small size. Since friction is proportional to the real area of contact, as well as the adhesion, the model can be called adhesion model. Direct dependence of friction on the normal force led to the recovering of 1^{st} Amonton's Law, but the assumption of totally plastic contacts is not realistic in normal machine,

since this would get completely damaged after some functioning time. Hence, elastic deformation had to be considered. They used then a simplified single asperity model of contact based on the Hertzian elastic theory, and found a non-linear friction-load dependence ($F_N^{2/3}$), which clearly contradicted Amontons 1^{st} Law and the experiments conducted at that time It was Archard (1953), who recognized that there was no contradiction between an elastic single asperity model and Amontons 1^{st} Law that is actually based on a contact involving many asperities [10]. Instead of assuming a constant number of asperities as Bowden and Tabor did, Archard assumed a load dependent number of asperities. With this assumption the controversy between the elastic multiple asperity hypothesis and Amontons 1^{st} Law could be resolved. Greenwood and Williamson further improved the method with a Gaussian and exponential distributions of asperities [11]:

$$F_F = \sigma A_R = \sigma \gamma F_N, \tag{1.2}$$

where $\gamma = A_R/F_N = (4\sqrt{\pi}/3)D\sqrt{\beta/\sigma}$. The asperities considered have the same radius of curvature β. D is the "inverse stress modulus" acting on the asperities. As it can be seen, the real contact area is proportional to the load and independent of the normal contact area. With the inception of the atomic force microscope and friction force microscope Bowden and Tabor's single asperity elastic theory, $F_N^{2/3}$, could be experimentally verified [12].

The classical tribometer experiments are essentially based on a slider moving over a surface. These tools were far insufficient to gain new insights of such an old but complex phenomenon as friction. But many things have changed in the last twenty years, as the progress of science led to new advanced methods and experiments able to performed improved studies of friction and wear. Frictional force microscope (FFM)[13], surface force apparatus (SFA)[14] and quartz crystal microbalance (QCM)[15] are the available tools for the scientists in their efforts to clarify several aspects of the sliding process of two surfaces.

The ultimate goal is to understand friction down to atomic scale, the sliding between two single asperities, as atomic friction is seen as an elementary process. The connection between atomic and microscopic friction is also the dream of many researchers.

1.2 Friction on the atomic scale

In order to understand the behavior of two real surfaces in relative motion while still in contact, many researches look down to the single-asperity level. There are several models based on continuum mechanics which predict how friction force should scale with the normal load. The Hertzian point contact model considers a fully elastic contact of two spheres, and predicts that the friction force scales

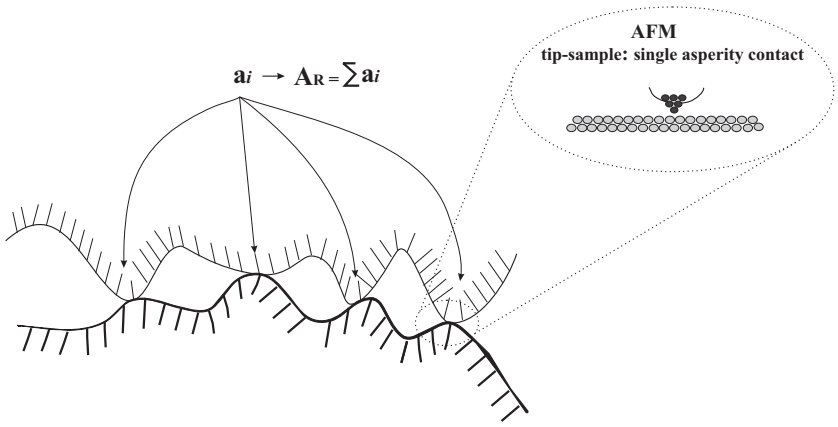

Figure 1.1: The real contact area of two surfaces consists of large number of small asperities, therefore it is much smaller than the apparent area of contact. Interaction of single asperities is now possible due to the invention of the AFM.

as $F_N^{2/3}$ [16]. Johnson et al. [17, 18] extended the Hertzian model taking into account the adhesion (JKR model). The contact radius a of A_R rigid sphere in contact with a compliant elastic half space depends on the work of adhesion $\Delta\gamma$:

$$A_R(F_N) = \pi(DR)^{2/3}(F_N + 3\pi\Delta\gamma R + \sqrt{6\pi\Delta\gamma F_N + (3\pi\Delta\gamma R)^2})^{2/3}, \qquad (1.3)$$

where R is the radius of the sphere, and D describes the elastic moduli and Poisson's numbers of sphere and the plane. Upon application of a negative load, the separation of the surfaces would occur for a pull-off force $F_{N(pull-off)} = -(3/2)\pi\Delta\gamma R$, independent of D, but dependent only on the radius of the sphere and the work adhesion. This model assumes that the attractive forces are confined to the contact area and are zero outside the contact area. Bradley modelled two rigid spheres considering only the adhesion but no deformation [19]. The model by Derjaguin, Muller and Toporov (DMT) [20], on the other hand, assumes that the contact area does not change due to the attractive surface forces and remains the same as in the Hertz theory. In this model the attractive forces are assumed to act only outside of the contact area. Due to the involved assumptions, the JKR model is more suitable for soft materials and the DMT model is more appropriate for harder materials. The Maugis-Dugdale (MD) theory is a generalization of all the above mentioned models. In all of them friction scales nonlinearly with the normal load, in contradiction to the linear behavior of the macroscopic friction.

With the birth of the atomic force microscope (AFM) and friction force microscope (FFM), the 2/3 power law predicted by single asperity elastic theory could be experimentally verified. The first observation of atomic friction processes was reported for a tungsten tip sliding over a graphite surface by Mate et al. [13]. A

rather linear dependence of friction on the applied load was found with a friction coefficient of about 0.01, which was explained by a multiasperity contact for high normal loads. Putman et al. observed the 2/3 power law in case of Si_3N_4-tip under humid condition, but a linear dependence under dry condition [21]. They claimed that the water film formed between tip and sample led to a smoother surface, which was acting as a single asperity. Schwarz found also linear and non linear behaviors on C_{60} and, respectively on GeS in air [22]. Carpick et al. studied the sliding of a Pt coated tip with different geometries over a stepped $SrTiO_3(305)$ surface [23]. For the analysis of lateral force vs. normal load an extended JKR model, taking the tip profile into account, was used. Enachescu et al. determined the load dependence of the contact area in ultra-high vacuum (UHV) for a hydrogen-terminated diamond(111)/tungsten carbide interface [24]. The extremely hard single asperity contact was described by the Derjaguin-Müller-Toporov continuum mechanics model. The variation in friction force with applied normal force was found to follow the variation of the contact area predicted by the Maugis-Dugdale theory in the case of a silicon tip on a $NbSe_2$ sample in UHV [25].

Another model used in describing friction of single asperity contacts is the Tomlinson model. It defines a fundamental mechanism of energy dissipation from an atom dragged across a periodic atomic lattice and is often used to model the dynamics of friction force microscope tips.

1.3 Tomlinson model

The development of scanning probe and UHV techniques allows today the evaluation of friction down to atomic scale [26, 27]. The motion of an AFM tip over the surface is often intermittent, with alternative sticking and sliding. Measurements of atomic scale friction by atomic force microscopy show generally a periodic variation of the lateral force with the lattice spacing of the surface being scanned, and having a saw-tooth shape characteristic of *stick-slip* motion. More details about this operating mode (contact-mode) of an AFM are presented in chapter 2.2. The atomic stick-slip mechanism is also the main source of dissipation in friction, the alternation between sticking and sliding states reflects changes in the way the energy is stored in the system. Theoretical studies of stick-slip aiming to interpret the FFM patterns [28, 29, 30, 31, 32, 33] on atomic scale are based on the Tomlinson model [34]. This paragraph describes in detail the friction process in the framework of the Tomlinson model in one-dimension, without taking into account thermal effects. The cantilever and the deformable contact between tip and sample can be seen as two springs in series (fig. 1.2). The effective stiffness

of this system is:

$$k_{eff} = (\frac{1}{k_{con}} + \frac{1}{k_T})^{-1}, \tag{1.4}$$

where k_T is the torsional spring constant of the cantilever, and k_{con} is the contact stiffness.

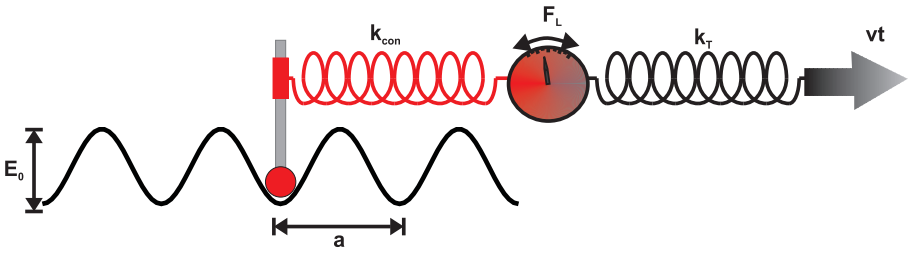

Figure 1.2: Effective stiffness of the system describing the force sensor in contact with the sample.

The tip of an AFM working in contact mode is the subject to tip-sample interaction potential and to elastic deformation of the cantilever. In a first approximation, the first potential can be assumed to have a sinusoidal shape and the second contribution is described by a parabola. In this case, the entire tip-sample interaction can be written:

$$V_{tot}(x,t) = -\frac{E_0}{2}\cos\frac{2\pi x}{a} + \frac{1}{2}k_{eff}(x - vt)^2, \tag{1.5}$$

where E_0 is the peak to peak amplitude of the sinusoidal potential, a is the atomic periodicity of the surface lattice, k_{eff} is effective stiffness of the tip-sample contact, and v is the constant velocity of the support, fig. 1.3.

At the moment t the tip is located in the equilibrium position $x{=}x_{min}$, obtained when the first derivative of V_{tot} with respect to x is zero:

$$\frac{dV_{tot}}{dx} = \frac{\pi E_0}{a}\sin\frac{2\pi x}{a} + k_{eff}(x - vt) = 0. \tag{1.6}$$

Using the approximation $\sin(x) \approx x$ in the equation 1.6, the initial velocity of the tip $(t \to 0)$ can be calculated:

$$\frac{dx_{min}}{dt}(t \to 0) = \frac{v}{1+\eta}, \tag{1.7}$$

where,

$$\eta = \frac{2\pi^2 E_0}{k_{eff}a^2}. \tag{1.8}$$

The coefficient η is the ratio between the strength of the tip-sample interaction and elastic energy of the system [35]. Using the same values of E_0, k_{eff}, a, v as

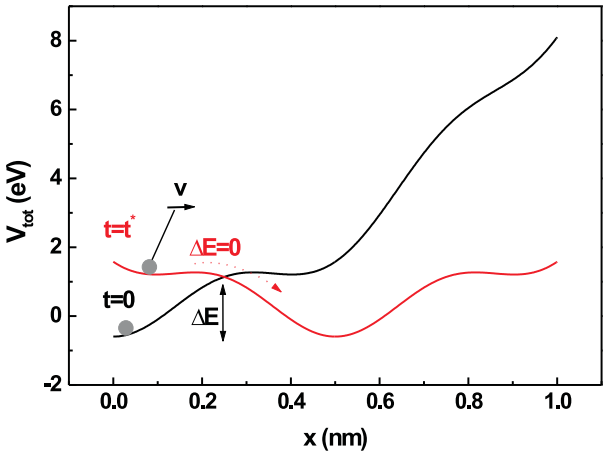

Figure 1.3: Total tip-sample energy interaction at the moment t=0 and at t=t^*. V_{tot} is calculated for E_0=1.22 eV, system tip-sample stiffness k_{eff}=2 N/m, atomic periodicity of the sample a=0.5 nm, and scan velocity v=50 nm/s.

for plotting V_{tot} in fig. 1.3, η gets a value of 7.49 and the initial velocity of the tip is 5.88 nm/s, much smaller than the constant support velocity $v = 50$ nm/s. The initial minimum position of the tip is increasing with time due to the motion of the cantilever until it becomes unstable. This is the moment $t = t^*$.

The critical position x^* corresponding to t^* is found when the second derivative of the total potential with respect to x is zero:

$$\frac{d^2V_{tot}}{dx^2} = \frac{2\pi^2 E_0}{a^2}\cos\frac{2\pi x}{a} + k_{eff} = 0, \tag{1.9}$$

leading to:

$$x^* = \frac{a}{2\pi}\arccos(-\frac{1}{\eta}). \tag{1.10}$$

At the moment t^* and at the position x^* an instability occurs and the tip *jumps* to the next minimum position of the potential profile. This kind of movement is called *stick-slip*. The lateral force $F^* = -k_{eff}(x^* - vt)$ in the moment of the jump can be evaluated from eqs. 1.6 and 1.9 using the fact that $\cos^2(x) + \sin^2(x) = 1$:

$$F^* = \frac{k_{eff}a}{2\pi}\sqrt{\eta^2 - 1}. \tag{1.11}$$

This force has a physical meaning only if $\eta^2 - 1 \geq 0$. Thus, the movement of the tip over the surface depends on the ratio between the two terms counting for the total interaction. The stick-slip behavior is possible only for $\eta > 1$; this being the case of a strong tip-sample interaction or a soft cantilever. With the values of η and a introduced above, the position when the tip *jumps* and the lateral force at

that position can be calculated: x^*=0.135 nm and $|F^*|$=1.18 nN. The moment of the instability can be consequently deduced: t^*=14.5 ms.

The lateral force due to the sliding of the tip over the surface is $F_L = -k_{eff}(x_{tip} - vt)$. A numerical evaluation of the lateral force leads to a behavior as in fig. 1.4. F_L reveals two opposite sawtooth profiles related to both direction of movement (forward and backward), and it is modulated with the same periodicity as the atomic structure of the underlying sample. The area enclosed in this hysteresis loop is a measure of the dissipated energy during the process of sliding [29]. When $t \to 0$ the lateral force is given by :

$$F_L(t \to 0) = \frac{\eta}{\eta + 1} k_{eff} vt. \tag{1.12}$$

When $\eta \gg 1$, the effective lateral spring k_{eff} is approximatively estimated by the ratio $|F_L(t \to 0)|$ / vt, as it can be seen in fig. 1.4.

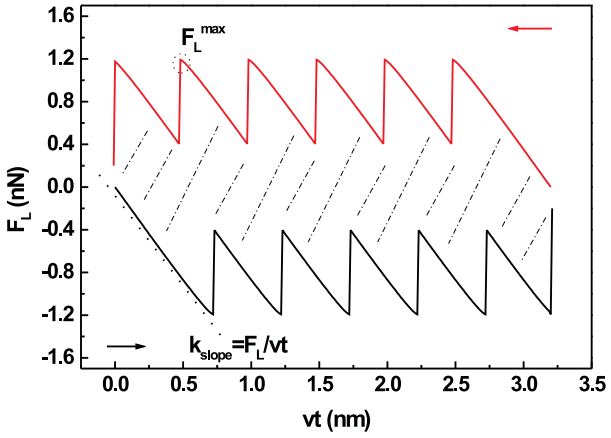

Figure 1.4: Lateral force between the tip and sample calculated according to Tomlinsom model for E_0=1.22 eV ($\eta = 7.49$), k_{eff}=2 N/m, atomic periodicity of the sample a=5 Å, and scan velocity v=50 nm/s. The black and red curves correspond to lateral force during the forward and respectively, backward movement of the tip over the surface.

The corrugation of the surface potential E_0 is linearly related to the maximum of the lateral force F_L^{max}. This can be found by analyzing the conditions for the position of the tip, eq. 1.6. Considering $F_L = -k_{eff}(x_{tip} - vt)$, it follows that:

$$F_L = \frac{\pi E_0}{a} \sin(2\pi \frac{x_{tip}}{a}). \tag{1.13}$$

The maximum of the absolute value of the lateral force F_L^{max} is found at x_{tip}=$a/4$, and E_0 becomes:

$$E_0 = \frac{aF_L^{max}}{\pi}. \tag{1.14}$$

Another important parameter in this model is $\Delta E(t)$, defined as the energetic barrier which should be overcome by the tip in order to jump from one minimum position to the next one: $\Delta E(t)$=$V(x_{max}(t), t) - V(x_{min}(t), t)$. If initially, at $t = 0$, the barrier energy encountered by the tip is ΔE, as depicted in Fig. 1.3, at the critical moment $t = t^*$ the cantilever has stored enough energy for jumping and $\Delta E(t^*)$ vanishes. The fact that $\Delta E(t)$ tends to zero at the critical point is trivial; taking into account eq. 1.6, one gets:

$$\frac{dE}{dt}(t^*) = k_{eff} v (x_{max} - x_{min}) = 0, \tag{1.15}$$

because x_{max}=x_{min} at the critical point. At finite temperature the barrier at x_{max} can be reduced and the slip probability becomes non-zero.

Two-dimensional Tomlinson model. More realistic, a point-like tip is moved along a two-dimensional sinusoidal potential. The Tomlinson model can be extended into two dimensions. The combined interaction potential becomes:

$$E_{tot}(\vec{r}, t) = V(\vec{r}) + \frac{k_{eff}}{2}(\vec{v}t - \vec{r})^2, \tag{1.16}$$

where $\vec{r}$ corresponds to x in one dimension, and $\vec{v}$ is the velocity of the tip arbitrary oriented on the surface. The periodic interaction potential can be rewritten:

$$V(x, y, t) = -\frac{E_0}{2}(\cos\frac{2\pi x}{a} + \cos\frac{2\pi y}{a}) + E_1 \cos\frac{2\pi x}{a}\cos\frac{2\pi y}{a}. \tag{1.17}$$

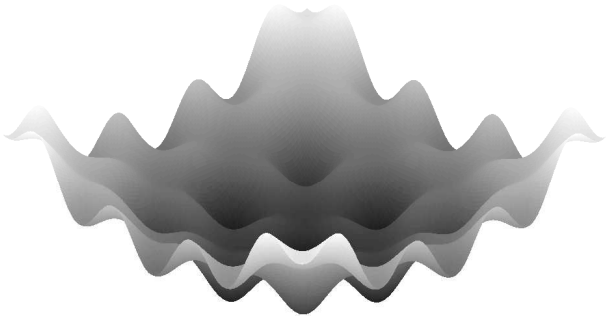

Figure 1.5: Total energy experienced by the tip in 2D model.

In this case the total energy can be represented as in fig. 1.5. The equilibrium position is achieved when:

$$\nabla_r E_{tot}(r,t) = \nabla_r V(r) + k_{eff}(\vec{r} - \vec{v}t) = 0, \tag{1.18}$$

and it is stable for positive eigenvalues of the Hessian matrix:

$$H = \begin{pmatrix} \frac{\partial^2 V}{\partial x^2} + k_{eff} & \frac{\partial^2 V}{\partial x \partial y} \\ \frac{\partial^2 V}{\partial y \partial x} & \frac{\partial^2 V}{\partial y^2} + k_{eff} \end{pmatrix}. \tag{1.19}$$

Each point in the $\vec{r}$ plan can be correlated to an eigenvalue with a certain sign. The landscape of the eigenvalues is presented in fig. 1.6. The tip follows the support adiabatically as long as it remains in a (++) region. When the tip reaches the border of these regions, it suddenly jumps into the next adiabatic region [29, 36].

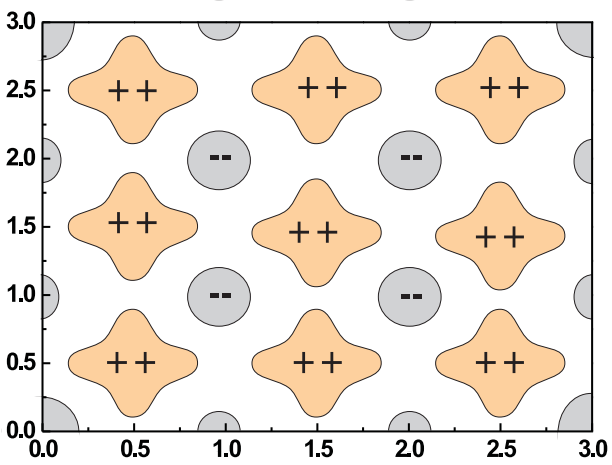

Figure 1.6: The region in the tip plane are labelled according to the sign of the eigenvalues of the Hessian matrix. The (++) regions correspond to an adiabatic movement of the tip, from the border of these regions the tips jumps to the next (++) domain.

1.4 Anisotropy of friction

Past measurements have shown that friction and adhesion between crystalline materials can be anisotropic in the sense that they depend on the relative crystallographic orientations of the two surfaces [37, 38]. Anisotropy was related to the incommensurability of the overlapping crystal surface lattices. In a such contact, the ratio between the lattice units of the two bodies along the sliding direction is irrational and different amounts of force pointing in any direction act on individual atoms. These forces consequently cancel each other and sum up

zero [39, 40, 41]. According to Hirano even a state of vanishing friction can be encountered when two solid in contact past over each other. The regime of zero friction force was called *superlubricity* [42]. He noticed a reduction of friction in scanning tunneling experiment with a tungsten wire on a silicon surface. Some earlier experiments reported reduced friction on mica [37], or ultra-low coefficients of friction in the case of MoS_2 [43]. Again, the origin of the noticed decreased or disappearance of friction was related to the incommensurate contact between the silicon tip and the surface. Dienwiebel et al. [44] used the term of friction anisotropy to describe the variation of friction on graphite with respect to the sliding direction, but not for the variation of friction as function of commensurability. For this experiment they built a dedicated instrument called Tribolever, which allows quantitative tracking of the forces on a scanning tip in three dimensions, with a resolution of lateral forces down to 15 pN [45]. A flake from the graphite surface was picked up by the Tribolever, and lateral forces between the flake and the surface were measured as a function of rotation angle. When the flake and the surface were rotated out of registry, to intermediate angles between 0° and 60°, the friction loops quickly reduced in amplitude, resulting in a smooth sliding with negligible friction. These results on graphite have led to the speculation that the excellent lubrication properties on graphite powder may be the result of superlubricity, the sliding actually taking place between misaligned graphite flakes, therefore leading to ultra-low friction. Severe reduction in friction was previously observed on different types of materials. Frictional contrast on a triglycine sulfate (TGS) surface was shown to depend on the sliding direction, the variation in friction being caused by an alternating tilt of TGS molecules in two domains of the substrate [46]. A peculiarity of TGS is that the arrangement of the molecules is rotated with 180° for two adjacent terraces. Overney et al. observed friction anisotropy on barbituric acid lipid [47] as in the case of TGS. There are other organic bilayer films presenting anisotropic frictional properties on different direction of scanning due to different molecular alignments in the substrate [48, 49, 50].

Beside commensurability another essential condition in achieving the zero state of friction is the dimensionality of interface and solids. If two chemically passivated and flat surfaces in contact are infinite, they slide without no resistance in motion [51, 52, 53]. M*ü*ser considered that the superlubricity term is inappropriate because the emission of sound waves occurs even in the absence of the instabilities leading to friction, a drag force linear in velocity. Therefore, he proposed a more fortunate term, *structural lubricity*, as the low friction arises mainly from the structural incompatibilities on the two contacting solids.

A totally different way to achieve decrease of friction is based on the Tomlinson model. This one describes a state of zero friction for single sliding asperities that could be well applied for studying an AFM tip in contact with the surface. In this case, the "superlubricity" is achieved without taking any assumptions about the contact size, hardness of the lattices, or commensurability of the interface. The

vanishing friction concept, together with some experimental proof of this theory are discussed in chapter 3.

A completely different approach for *tuning* the frictional response, which recently has attracted considerable interest [54, 55, 56], is to control the system mechanically via normal vibrations of small amplitude and energy. In this case, the idea is to reduce the friction force or to eliminate the stick-slip motion through an excitation of vibrational modes. Calculations demonstrated that oscillations of the normal load could lead to a transition from a state of high-friction stick-slip dynamics to a low-friction smooth sliding state. Manipulation by mechanical excitations, when applied at the right frequency, amplitude and direction, pull the molecules out of their potential energy minima and thereby reduce friction (at different frequencies or amplitudes the friction can alco be increased). The results presented in chapter 4 show how an ultra-low regime of friction or even zero energy dissipation can be achieved in atomic scale motion by introducing a perturbation normal to the plane of sliding. Excitations of the cantilever or modulated bias voltage between tip and sample were applied. The decrease of friction was obtained only for perturbations with frequencies matching exactly the normal resonance frequency of the coupled tip-surface system.

1.5 Wear on the atomic scale

On the other hand, a completely different situation, the wear effect, can be encountered in tribology. This effect is in contrast to the ultra-low friction state, as it is accompanied by very high friction forces between two bodies in contact and by the damage of at least one of the surfaces involved in the contact. If regimes of almost zero friction can be obtained in the manipulation of an AFM tip over a surface, the wear process can be also present in the AFM measurements if some conditions are met. With a careful manipulation of the normal load applied to the tip this extreme situation can occur, and the surface topography can be permanently modified. With a load exceeding a critical value, depending on the tip and sample's shape and nature, the underlying surface starts to be worn off. There are different experimental examples in which the FFM proved to be an useful tool for producing wear and imaging the damaged surface on atomic scale [57, 58]. These studies were performed on ionic crystals and proved that even well defined patterns could be created on such surfaces. Wear processes under the action of the AFM tip has been experienced on different kind of materials. The tip can worn off mica, removing sheets of this layered material for normal loads of hundreds of nanonewton [59]. Polymer films is another class of materials under investigation from the point of view of wear properties [60]. The formation of stable patterns was observed depending on the nature of the molecules, the ratio between inter-molecular and molecule-substrate interaction, and the deposition

conditions. The resulting structures were considered to be the effect of a peeling process operated by the tip [61].

Ripple formation due to perturbations acting on a surface is commonly observed on macroscopic scales. Well-known examples are given by wind-blown sand dunes observed in the desert and on the shore [62]. The dynamics of sand motion consist of two processes: the transfer of the sand grains from one position to another, and the movement of the sand along the surface without jumps. The combination of both results in the formation of regular dunes. Elastic instability waves were observed by Schallamach on macroscopic length scales for elastically soft materials, such as rubber during sliding on hard surfaces [63]. Self-organization of surface undulations have also been reported on the nanometer scale. For example, ripples are formed when glasses, amorphous films, semiconductors, or metals are sputtered by ion beams [64]. These features have typical wavelengths of few tens of nanometers, and they can be revealed by scanning probe microscopes. Leung and Goh observed the formation of ripples when the tip of an atomic force microscope was scanned over a polymer film [60]. The orientation of the ripples was perpendicular to the scan direction and their characteristic wavelengths were in the range between 10 and 100 nm. Ripples produced by scratching were observed on polymers several times, and, more recently, even on gold films [65]. The ripples were considered to be the result of a peeling process operated by the microscope tip in the case of polymer films [61], or as a result of a self-regulating periodic pickup and release of clusters in the case of gold films [65].

The understanding of wear is not so trivial. There are still unclear aspects for describing the tip sample interaction, the conditions for wear onset and how the debris is moved by the tip. All the methods and models based on the continuum mechanics are limited in describing the formation and the disruption of small and sliding contacts. Molecular dynamics (MD) came then as a tool for microscopic modelling of the contact, giving information about the tip sample interaction not accessible experimentally.

In case of ionic crystal surfaces MD shed some light on the sliding process down to atomic scale. Shluger et al. showed that there is a continuous transfer of atoms between the MgO tip and LiF(100) sample [66]. They claimed that a dynamic self-organization of the surface material on the tip might be a possible condition for observing periodic forces. This self-lubrication effect of the tip suggests a direct relation between friction and wear.

On metallic surfaces Sørensen predicted also wear processes [41]. An (111) terminated copper tip slides in a stick-slip fashion on Cu(111) surface, as described by the Tomlinson model, whereas adhesive wear was predicted in the case of the (100) tip. Sliding in the (011) direction at constant load or constant distance led to inter-plane sliding between (111) planes inside the tip. Abrasive wear is also reported in MD, for instance nanoindentations and sliding of a sharp tip Ni(111) tip on Cu(110) and of a blunt Ni(001) on Cu(100) [67]. In both cases the lateral force showed quasi-periodic variation, due to the stick-slip in-

volving phase transitions . Molecular dynamics simulations of nanoindentations followed by nanoscratching were conducted on single crystal aluminum with an infinite hard Ni tip [68]. In this study, whenever material removal is involved in atomic-scale friction even at extremely fine scratch depths, the magnitude of the friction coefficient is high, dependent on the rake angle presented by the tool, and independent of the normal force. Suresh et al. quantified two key features of wear process: 1) the nucleation and 2) subsequent the evolution of defects in crystals [69]. They present a fundamental framework for describing incipient plasticity that combines results of atomistic and finite-element modelling, theoretical concepts of structural stability at finite strain, and experimental analysis.

Having discussed some experimental and theoretical issues related to the tremendous efforts of understanding and describing the wear process down to atomic scale, we have performed furthermore wear measurements by means of an AFM on ionic crystals. Chapter 5 of this thesis mainely presents an analysis of wear on KBr(001), continuing traditional frictional studies on such materials in the group of Prof. Ernst Meyer. It will be shown how wear is initiated at nanometer scale, how the surface is worn off layer by layer and the debris reorganized in regular patterns under the action of the tip. The influence of the tip geometry, the environment and the nature of the studied surface are also topics of this chapter.

Chapter 2

Experimental set-up

All the experiments presented in this thesis were performed in the NANOLINO lab of Prof. Dr. Ernst Meyer by means of an atomic force microscope operated in ultra high vacuum.

2.1 Principle of AFM

The force microscope was designed to measure forces between a sharp tip and a surface. The tip is mounted at the end of the cantilever, whose deflection is related to the interaction force between tip and sample. Tip-sample interactions can be deduced from the static deflection of the cantilever or from its dynamical behavior. *Atomic Force Microscope* is an instrument able to detect forces down to the atomic scale, such as interaction forces between atoms. Our microscope is based on the beam deflection method. A light beam is reflected on the rear side of the cantilever. The deflection is sensed by a quadrant photodiode. A sketch of the setup is presented in figure 2.1. The four-segment photo diode allows to detect not only the normal bending but also the torsion of cantilever caused by lateral forces acting on the tip. The A-B-signal is proportional to the normal force and the C-D-signal is proportional to the torsional force. In our microscope the optical beam deflection detector and the sample position can be adjusted by three

stepping motors. The advantage of this detection is the long working distance between optics and the cantilever, that makes possible the in situ exchange of cantilevers. The whole AFM is mounted on a platform suspended by four springs and damped with efficient eddy currents. The vacuum system is divided into two parts:
1. The preparation chamber, in which the sample can be annealed and sputtered. Three Knudsen-cells are used for the deposition of different materials (molecules, metals, insulators) on clean surfaces. There is also a quartz microbalance able to calibrate these depositions.
2. The analyzing chamber is the place were the AFM measurements takes place. In this part there are few spectroscopic devices to characterize the samples, like Low Energy Electron Diffraction (LEED), Auger Electron Spectroscopy (AES) and Xray Photoelectron Spectroscopy (XPS).
Both chambers are under UHV conditions. The whole system is pumped by one Turbo-molecular-pump, and Ion-Getter-pumps and a Titanium-sublimation-pumps. The background pressure obtained in this way is around 10^{-11} mbar.

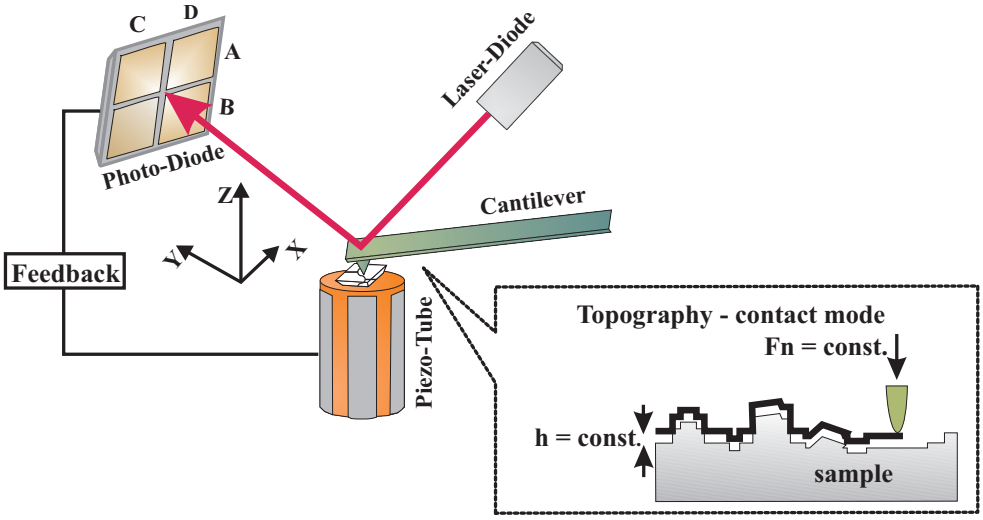

Figure 2.1: Schematic diagram of the beam-deflection AFM. A laser beam is deflected of the rear side of the cantilever. Angular deflections of the laser beam are measured with a position sensitive detector. The A-B-signal is proportional to the normal force and the C-D-signal is proportional to the torsional force.

The AFM can operate in static and dynamic modes, in which the static bending of the cantilever or its dynamic behavior are measured, respectively. The most important static mode and the one used for all the measurements in this thesis is the so-called *contact mode*. In constant force mode, the tip is constantly adjusted to maintain a constant deflection, and therefore a constant height above the surface. Fig. 2.1 sketches this mode of scanning. It is this adjustment that is

displayed as data. Topographic images can also be obtained by scanning the tip over the sample at constant height. The deflection is attributed to the normal force acting on the cantilever and can be calculated by multiplication with the spring constant of the cantilever. However, the ability to track the surface in this manner is limited by the feedback circuit.

More information about the nature of tip-sample interactions can be obtained by recording the desired signal (the normal deflection for contact mode) as a function of distance between tip and surface. The resulting *Force-distance curve* looks like in fig. 2.2. When the tip is brought in contact the attractive long-range forces between tip and sample are balanced by the short-range repulsive force and the external force exerted on the cantilever. The total normal force deduced from the bending of the cantilever is not only the difference between the normal load and repulsive forces, but the attractive forces should be added (adhesion). Repulsive forces increase strongly with the decrease of tip-sample distance. Therefore, images of constant repulsive force are often identified with topography.

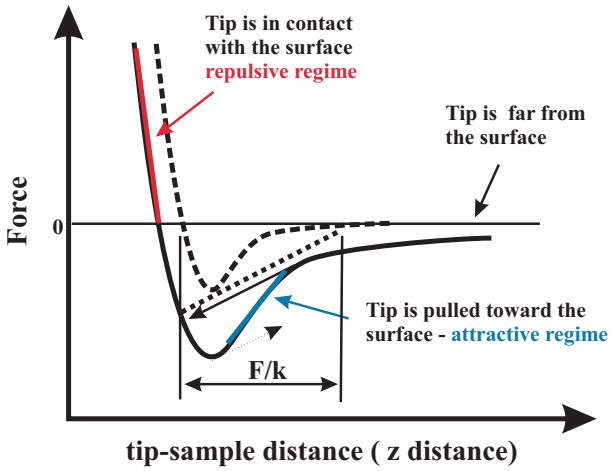

Figure 2.2: Cantilever bending versus tip-sample distance. The solid line is the total tip-sample force and the dashed line is the contribution of the short-range forces. The arrows indicate the jump into and out of contact and the dotted lines are linear funtionswith the slope of the spring constant of the contilever, k.

The resolution of the images in contact mode is limited to the atomic lattice, but not below. Single point defects were not observed so far. This drawback in sensing true atomic resolution is explained by the area of the tip-sample contact, which is larger than atomic distances.

2.2 Lateral Force Measurements by AFM

Our home-built UHV-AFM is able to measure not only the normal but also the lateral forces acting on the sensor tip by means of an optical beam deflection. As it was said before, the C-D-signal of the photodiode is proportional to the torsional force. When moving over a flat surface with zones of different friction forces, the angle of torsion will change in every new zone [70, 71, 72]. This allows measuring of the local friction force. Lateral friction contrast can be also caused by geometrical features like steps or holes [73]. To distinguish zones of different friction and exclude topographic effects one can utilize a second pass on the same scanning line, but in opposite direction. The comparison of both directions is necessary in order to avoid the cross-talk of the normal force into the lateral signal. If the cross-talk of the torsional bending is negligible, the topography images should be identical for forward and backward scan direction, while the lateral force maps are inverted due to the inverse sign of friction forces. In addition, the lateral force measuring mode easily provides the atomic resolution on different class of materials, like layered materials [74, 75] or non-layered ionic crystals [76, 77]. As discussed previously (ch. 1.3), the lateral force (F_L) measured by FFM on well defined surfaces can reveal atomic-scale features. The lateral force increases when the tip is locked to one atomic position until it becomes strong enough to provoke a slip of the tip into the next atomic position. Furthermore, the lateral force presents hysteresis while scanning in the opposite direction. From the area enclosed by the friction loop, the energy dissipated in the sliding process can be calculated.

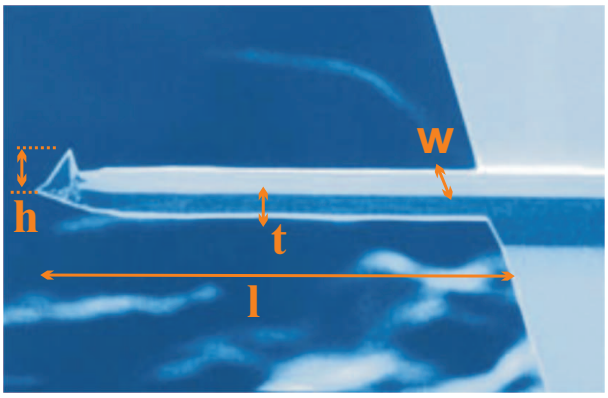

Figure 2.3: Rectangular cantilever used for force measurements with its relevant dimensions: length l, width w, thickness t and height h of the tip.

The cantilevers used in our experiments are made of silicon and are rectangular. Silicon cantilevers consist of single crystalline materials, the pyramidal tip is pointing toward the <100> direction and has a microscopic cone angle of 50°.

At the apex, the cone angle is reduced and tip radii of 10 nm can be obtained [78]. The tip apex radius and aspect ratio are crucial for the lateral resolution on rough surfaces, and also for the relation between short-range and long-range forces.

For quantitative interpretation of FFM images the normal and torsional bending of the cantilever have to be calibrated [57]. A scanning electron microscope (SEM) image of a cantilever and its relevant dimensions is presented in Fig. 2.3. The normal spring constant k_N is given by:

$$k_N = \frac{Ewt^3}{4l^3}, \tag{2.1}$$

where w is the width, l the length, t the thickness of the cantilever and E the Young modulus of the material. For silicon E=1.69x10^{11} N/m^2. The thickness can be precisely determined from the resonance frequency, f, of the cantilever:

$$t = \frac{2 \cdot \sqrt{12}\pi}{1.872^2}\sqrt{\frac{\rho}{E}} \cdot f \cdot l^2 = 7.23 \times 10^{-4}\frac{s}{m} \cdot f \cdot l^2, \tag{2.2}$$

where ρ is the mass density (silicon: ρ=2300 kg/m^3). The relation between the defection of the laser beam measured by the photodiode and the normal force acting to the tip can be obtained by recording deflection vs. distance curves (fig. 2.2).

The torsional spring constant k_T necessary for lateral force calibration is given by:

$$k_T = \frac{G\omega t^3}{3h^2 l}, \tag{2.3}$$

where G (silicon: G=0.5x10^{11} N/m^2) is the shear modulus.

Chapter 3

A new regime of super-low friction

3.1 Introduction

" *The ability to produce durable low-friction surfaces and lubricant fluids has become an important factor in miniaturization of moving components in many technological devices...*"

This statement is a good motivation for the work presented in this chapter. The question "Can two bodies slide past of each other without friction?" is one of the reasons of many tribological studies. The first materials that seem to show significant reduction of friction even in macroscopic sliding were the lamellar solids. Macroscopic friction involves many micro-contacts with different size and orientation. Negligible micro-scale friction has been observed on graphite, MoS_2, Ti_3SiC_2, known as good solid lubricants, and thus with wide practical applications [43, 79]. A recent proof of this idea is the work of Dienwiebel et al., who showed that friction between two graphite sheets is significantly reduced when the surfaces are rotated out of the commensurate locking angle [44]. The following speculation has been proposed: in the case of macroscopic lubrication by graphite

a large fraction of the graphite contacts will be in the "superlubric state", while only a small fraction will be in registry, thus explaining the tremendous reduction in the average friction force, experienced in the ensemble of micro-contacts. With a dedicated instrument, called Tribolever, it was able to obtain quantitative tracking of the scanning tip in three dimensions. Relative low coefficients of friction were found by means of an STM, using a tungsten tip sliding over highly ordered pyrolytic graphite under ambient conditions [13].

In the following section it will be proven that the state of zero friction can be achieved in a completely different way, independent of the material of the studied surface. Lamellar materials are not the only category of solids presenting "superlubricant" properties in sliding. It is also important how the reduction of friction is obtained and how this process can be controlled.

3.2 Theoretical non-dissipative regime

Superlubricity can also be achieved in a completely different way.

In the paragraph 1.3 the case of $\eta \gg 1$ has been analyzed, where parameter η is the ratio between the strength of the tip-sample interaction and the stiffness of the system. But trivial questions arise: What happens when η comes close to 1 or becomes even smaller than this value? What happens in the case of stiff systems or very weak tip-sample interaction when the elastic energy stored in the cantilever becomes equal or larger than the corrugation of the surface potential? The answer to these questions is the appearance of new mechanism of *ultra-low friction* between two solids sliding in contact. Opposite to the mechanism discussed just before, this one implies the motion of a single asperity over an array of atoms ordered in a crystal lattice. The tip can be seen as consisting of a single atom and its frictionless motion can be described in the frame of Tomlinson model, under the conditions $\eta \leq 1$.

Following the same procedure in evaluating the lateral force as in the paragraph 1.3, the friction loops for three values of η and for an effective stiffness of the system k_{eff}=1 N/m are presented in figure 3.1. For η=5 the lateral force reveals two separated sawtooth profiles for the two directions of scanning. The tip moves over the surface in a classical stick-slip fashion. The area enclosed in the hyteresis loop is the energy dissipated in one sliding cycle. If η=3 the lateral force shape is preserved but the two curves partially overlap. Friction changes its sign during the slip event. Similar cases are presented in the literature [80, 81], where the atom of the tip moves smoothly through a repulsive, then an attractive force field, first being repelled by, and then pushed by the lower substrate.

A totally different situation is met for η=1. In such cases, the hysteresis loop completely disappears. The two curves for the two direction of scanning coincide,

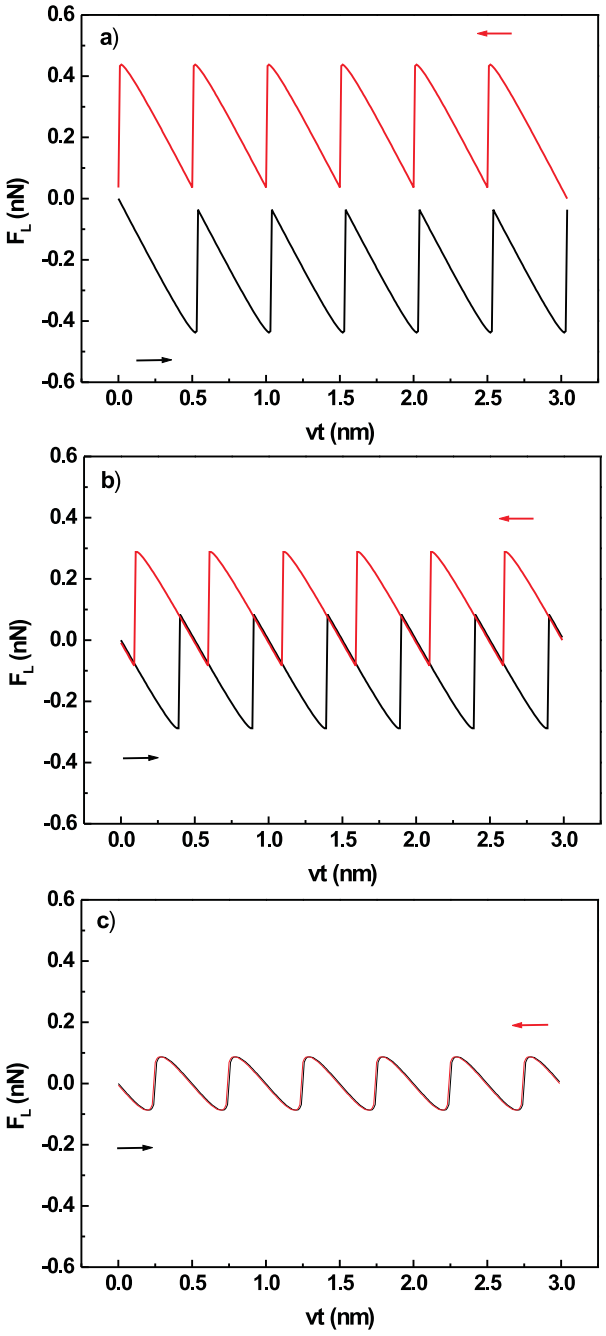

Figure 3.1: Lateral force between the tip and sample calculated accordingly to the Tomlinsom model for three values of η: a) η=5, b) η=3, c) η=1. System stiffness k_{eff}=1 N/m, atomic periodicity of the sample a=0.5 nm, and scan velocity v=3 nm/s. The black and red curves correspond to the lateral force during forward and backward movement of the tip over the surface.

giving an average friction force equal to zero. Zero friction implies that no energy is dissipated in the sliding process. The sawtooth modulation of the lateral force is transformed into a continuous modulation (almost sinusoidal) with the lattice periodicity. The value η=1 represents the threshold between a dissipative regime (η >1) and a new one, nondissipative. The slips are the main events responsible for dissipation on the atomic scale, but not the only ones. The damping of the two bodies in contact leads certainly to new channels of dissipation of several orders of magnitude smaller. With the assumption that the cantilever is damped by a viscus force γ, it's motion is given by:

$$m\frac{d^2x}{dx^2} + \gamma\frac{dx}{dx} - \frac{\pi E_0}{a}\sin\frac{2\pi x}{a} + k_{eff}(x - vt) = 0. \tag{3.1}$$

Since the contact spring has negligible mass, it will relax in a time of the order of that for a stress wave to traverse the contact diameter, of order of 10^{-12}s, which is much shorter than the natural period of the cantilever, 10^{-4}s. The strain released in this relaxation will be entirely dissipated in phonons [32]. Studies of dynamical behavior of FFM at T=0 using the Tomlinson model showed peculiar features in the case of a low viscous friction coefficient, bifurcation, chaotic motions, resonances at fractional, and multiple frequencies of the oscillator and hysteresis [82]. In most of the dynamical simulations, the critical damping, γ_{cr}=$2\sqrt{k_{eff}/m}$, has been assumed to suppress these abnormal behaviors. The damping of the system is given by the ration γ/m. Figures 3.2 shows how the tip moves over the atomically corrugated surface for different values of the damping at T=0. The mass of the cantilever was considered to be 8*10^{-12} Kg, the scanning velocity was 10nm/s and the parameter eta was chosen to be equal to 5.

It can be seen that single or double slips can be encounter in sliding friction depending on the damping of the system. In figure 3.2 the system find the minimum in the faster manner when is critically damped. If the damping is further decreased significant oscillation appears after the slip motion, and even more the slip motion changes to double slips. The double slips occur if the tip atoms can arrive at the next nearest local minimum, overcoming the middle energy barrier in between. The irregular mixing of double slips was also observed on graphite at a high load [13]. The existence of regular double slips had been pointed out already [32, 83]. It's worth to mention that in practical experiments, irregular mixing of double slips among single slips was observed on mica at high sliding velocities while regular single slips were observed at low velocities [84]. However, both the appearance condition of double slips and the mechanism of the irregular mixing of single and double slips has not been fully resolved yet.

In condition conditions of $\eta \leq 1$ some corrections should be made in evaluating parameters of the Tomlinson model. 1.12 gives the relation between F_L and position of the support of the tip (vt) at the beginning of each sticking phase. $\frac{F_L}{vt}$ is equal to k_{eff}, and implicitly to the slope of the sticking part of the friction profile only if $\eta \gg 1$. In general, k_{slope} (F_L/vt, fig. 1.4)is not equal to k_{eff}, but:

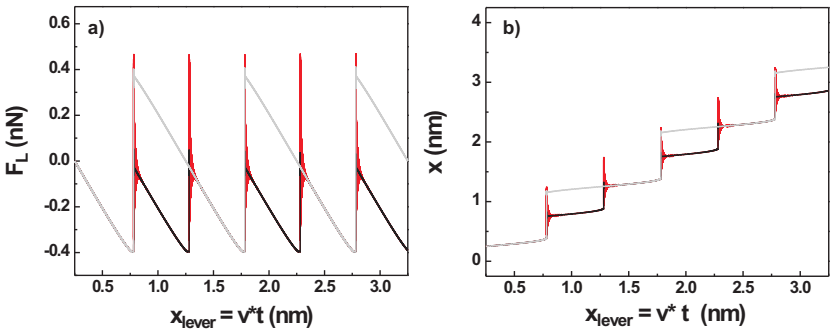

Figure 3.2: a) Lateral force between the tip and sample and b) position of the tip with respect to the lever position, calculated accordingly to the Tomlinsom model for three $\eta = 5$ and three different value of γ. System mass was m =$8{*}10^{-13}$ Kg, system stiffness k_{eff}=1 N/m, atomic periodicity of the sample $a = 0.5$ nm, and scan velocity $v = 10$ nm/s. The black curves are obtained for γ_{cr}, the gray curves for $\gamma_{cr}/10$, and the red ones for $\gamma_{cr}/100$.

$$k_{slope} = \frac{\eta}{\eta + 1} k_{eff}. \tag{3.2}$$

From eqs. 1.8, 1.14, 3.2 the effective stiffness of the tip-sample assemble could be estimated:

$$\eta = \frac{2\pi F_L^{max}}{k_{slope} a} - 1, \tag{3.3}$$

where F_L^{max}, k_{slope} are values accessible in experimental measurements. In this conditions, parameter η delimiting the transition from stick-slip behavior to a continuous sliding of the tip becomes an important challenge for experimentalists for achieving the *ultra-low friction* regime in atomic friction.

3.3 Lateral force measurements on NaCl

The regime of zero friction, theoretically described in section 3.2, can be also achieved experimentally, independent of the nature of the involved surface, if the parameters that determine the value of η can be tuned correctly. In the experiment discussed in this part η is reduced by decreasing the amplitude of the tip-sample interaction potential via variation of the normal load.

Typical lateral force measurements look like in fig. 3.3a) with clear differences for both directions of scanning. The movement of the tip is clearly of stick-slip type: the tip sticks in each minimum atomic position till the energy stored in the

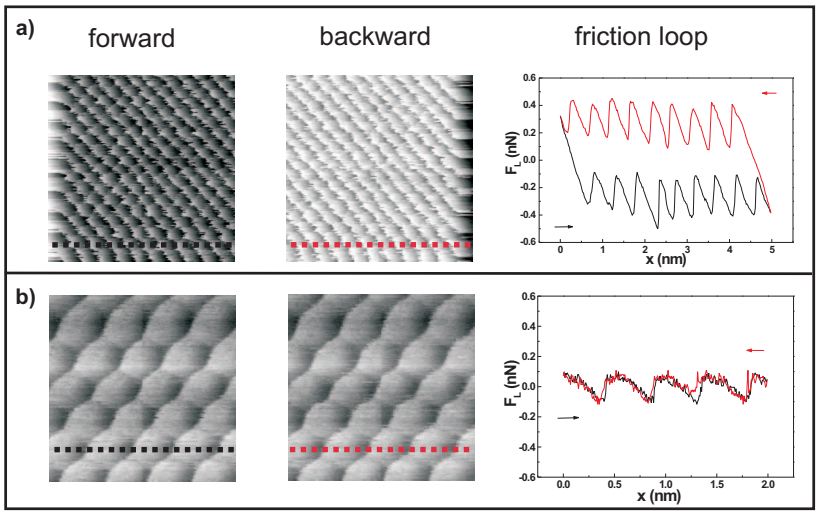

Figure 3.3: Lateral force between a silicon tip and NaCl(001) sample for two values of normal force applied. Friction force map a) is obtained for F_N=0.44 nN and the energy dissipated per slip is E_{diss}=1.4 eV. In case b) the load is F_N=0.14 nN and $E_{diss} \ll$0.1 eV.

cantilever is high enough to make the tip jump to the next minimum position. The total energy dissipated in the sliding process is in this case 1.4 eV per slip event. Decreasing the normal force applied on the tip, a different kind of friction map was achieved (fig. 3.3b). The friction loop leading to dissipated energy in the sliding process of two bodies in contact disappeared. Within the limit of the sensitivity of our instrument the dissipated energy per slip was evaluated less than 0.1 eV . Practically, the tip and sample slide over each other with almost no friction.

3.3.1 Why ionic crystal surfaces are "ideal" for friction measurements?

In ambient conditions there is always a thin layer of contaminants, like water, hydrocarbons present on the surface but also on the tip. Surface irregularities, cracks, pores can be filled and covered due to the capillary condensation of water or any other contaminants. In order to exclude the influence of contaminants, many friction experiments are conducted in UHV [21, 85]. The goal is to perform wear-less friction measurements on the atomic scale and on clean surfaces and to approach the case of single asperity contact between tip and sample. The ionic crystals were the subject of many FFM studies [57, 86, 87, 88]. They are insulating materials and have one of the simplest atomic structures. The anions

and cations held together by electrostatic interaction and they can be treated as impenetrable charged spheres. The alkali halides can be regarded as ideal ionic crystals. Under normal conditions they are cubic and the majority crystallizes in the NaCl structure. The natural cleavage plane is (001). In the actual study we have chosen NaCl with the lattice spacing 5.6 Å, especially for its simplicity and weak interaction with the tip [89].

3.3.2 Results of lateral force measurements

Here, the first experimental observation of the transition from stick-slip to continuous sliding in atomic friction is reported. The first mechanism is characteristic for the friction of two bodies in contact, the latter is inherently linked to a regime of ultra-low dissipation. The measurements were realized with our home built friction force microscope operated at room temperature and under ultrahigh vacuum condition (section 2.2).

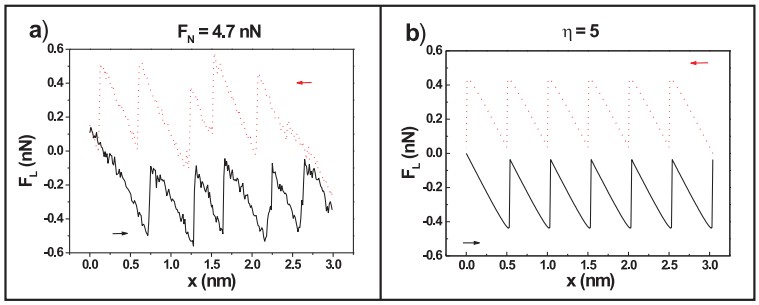

Figure 3.4: a) Measurements of the lateral force acting on the tip sliding forwards and backwards in (100) direction over the NaCl(001) surface. Cross-section through a two-dimensional scan obtained for an external load F_N=4.7 nN. b) Corresponding numerical evaluation of F_L from the Tomlinson model for η=5.

Silicon cantilevers with a spring constant of $k_N = 0.05$ N/m for normal bending and $k_T = 29$ N/m for torsion were used. The radius of curvature of the tip was nominally below 15 nm (section 2.2). The feedback loop controlling the tip-sample distance was operated very slowly, in order to avoid any influence of the feedback on the measurement of the lateral forces. The experiments were performed on NaCl single crystals cleaved in UHV and heated at 150° C to remove charges produced in the cleaving process. The normal and lateral forces acting on the tip were calibrated according to the procedure given in Ref. [90].

Fig. 3.4a, 3.5a, 3.6a show the lateral force F_L recorded with three different externally applied normal loads F_N. The total normal force between tip and surface is the sum of the externally applied load and the attractive force between

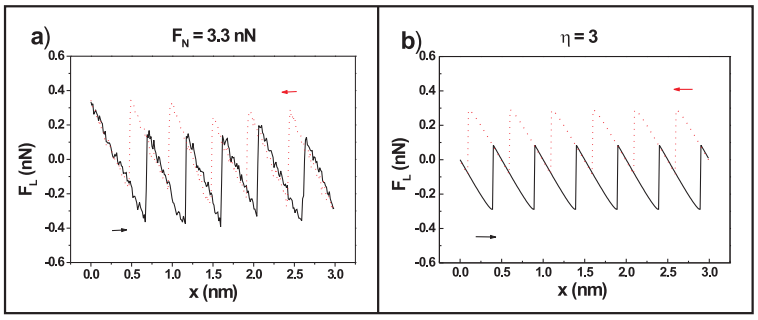

Figure 3.5: a) Measurements of the lateral force acting on the tip sliding forward and backward in (100) direction over the NaCl(001) surface. Cross-section through a two-dimensional scan obtained for an external load F_N=3.3 nN. b)Corresponding numerical evaluation of F_L from the Tomlinson model for η=3.

tip and sample. The latter has been determined to be 0.7 nN by measuring the force required to pull the tip out of contact. The scan velocity was $v = 3$ nm/s.

For $F_N = 4.7$ nN the lateral force reveals two opposite sawtooth profiles when scanning forwards and backwards (Fig. 3.4a). The sawtooth modulation has the periodicity of the crystal lattice along the (100) direction and is characteristic for the stick-slip process. The area enclosed in this hysteresis loop is the energy dissipated in one cycle.

When the externally applied load is lowered to 3.3 nN the dissipated energy decreases, while the amplitude of the sawtooth modulation stays constant resulting in an overlap of the curves for the forward and the backward scan. In fact, the lateral force changes its sign in the slip event (Fig. 3.5a). While the moving spring is pulling on the contact before the slip, the contact is pulling on the spring after it has slipped to the next atomic position and, thereby, has surpassed the moving support of the spring. A similar load dependence of the stick-slip behavior has been observed, as we discussed before, on the layered materials graphite and MoS_2 but for normal loads of higher orders of magnitude [13, 27].

A completely different picture is found when the load is further reduced. For normal loads below a certain threshold, the hysteresis loop and with it the dissipation disappears within the sensitivity of the current experiment (Fig. 3.6a). The sawtooth modulation of the lateral force is transformed into a continuous modulation of perfect match between forward and backward scan, still showing the atomic periodicity of the surface lattice.

The observed transition can be explained in a classical one-dimensional Tomlinson - type model, as explained in sections 1.3, respectively 3.2. Next to the friction loops presented there are the corresponding theoretical loops obtained for different values of the parameter η (eq.1.8). Numerical results for three different values of η are presented in Fig. 3.4b, 3.5b, 3.6b. The movement of the tip from

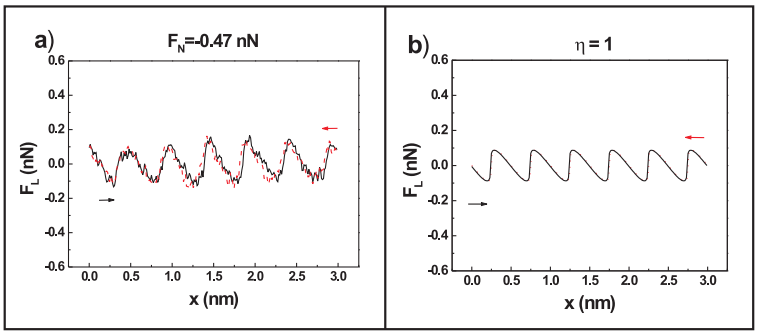

Figure 3.6: a) Measurements of the lateral force acting on the tip sliding forward and backward in (100) direction over the NaCl(001) surface. Cross-section through a two-dimensional scan obtained for an external load F_N=-0.47 nN. b) Corresponding numerical evaluation of F_L from the Tomlinson model for η=1.

one minimum position to the next can be continuous or jumping, depending on the relation between corrugation E_0 and elastic energy which can be described by this parameter. When $\eta < 1$ the movement is continuous and no dissipation occurs (Fig. 3.6b), when $\eta > 1$ the stick-slip behavior is found (Fig. 3.5b and 3.4b).

3.3.3 Friction versus load

Naturally, the next step is to discuss the relation between the experimentally accessible F_N and the theoretical η parameters. We demonstrate how η can be tuned by varying the normal load on the contact. Experimentally, the dissipation or, correspondingly, the mean friction force decreases by reducing normal load and reaches zero before the sliding tip jumps out of contact. In the model, the dissipation decreases for decreasing η and is zero for all values $\eta \leq 1$. These two dependencies are compared in Fig. 3.7. The similarity of the two curves bring us to the question, in how far the parameter η of the Tomlinson model is accessible to the experiment via variation of the normal load. In order to answer the question, we try to calculate all parameters of the Tomlinson (E_0, η, k_{eff}, k_{slope}) model by a detailed analysis of the experimental data.

3.3.4 Corrugation of the surface potential

According to eq. 1.14, the corrugation of the sample felt by the tip depends on the the maximum absolute values of the lateral force F_L^{max}, measurable from the maxima of curves like those in Fig. 3.4a, 3.5a, 3.6a. The load dependence

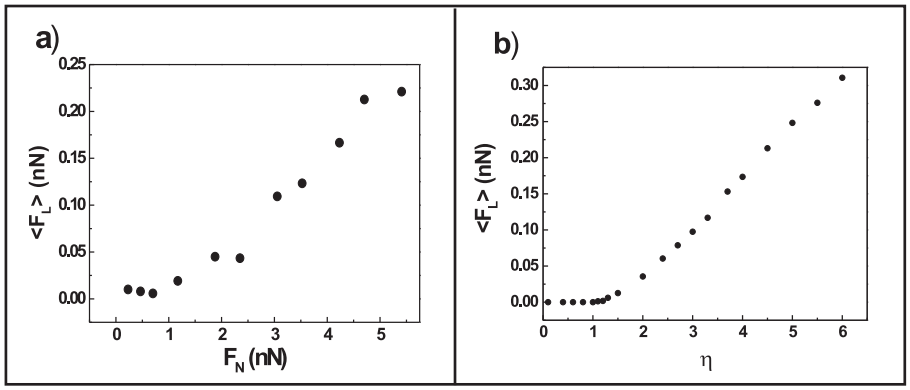

Figure 3.7: a) Mean lateral force versus normal load. The experimentally determined adhesion has been added to the externally applied load. The data points represent the average over a two-dimensional scan of 3x3 nm^2. b) Numerical evaluation of the mean lateral force as function of η in the one-dimensional Tomlinson model. Quantitative difference between experimentally and numerically obtained forces can result from the two-dimensional averaging in the case of experimental results. The numerical results have been calculated for lines with maximal corrugation, like those presented in part b) of figures 3.4, 3.5, 3.6.

of the potential corrugation E_0 is shown in Fig. 3.8. The corrugation of the surface potential E_0 is linearly related to the maximum lateral force F_L^{max}. The increase of the corrugation height of the potential with increasing normal load can be intuitively understood as an increase of the barrier height between adjacent atomic positions when the contacting atoms are pressed closer towards the surface lattice. For a different atomic system it has been confirmed in a first principles study [28].

Experimental determination of E_0 were done first time by Riedo et al. performing measurements on freshly cleaved and atomically smooth muscovite mica surface in controlled humidity environment [91]. They found similar values for the surface corrugation and even a linear dependence with the external normal load applied. The friction force on a tip sliding on a surface was related to the thermally activated hopping of the contact atoms on an effective atomic interaction potential. They experimentally and theoretically found a velocity which marks the transition from logarithmic increase of $F_L(v)$ to a region where friction is constant since thermal activation ceases to be relevant. This velocity is analytically related to the potential corrugation, E_0.

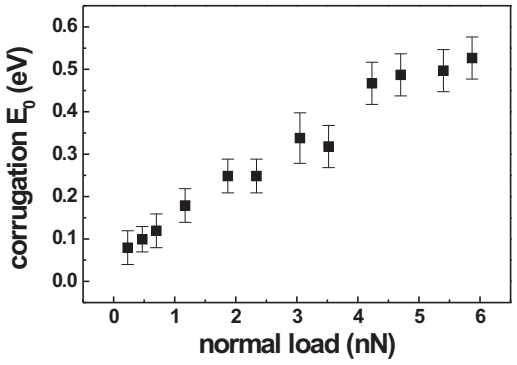

Figure 3.8: Energy corrugation E_0 as function of the normal load F_N acting on the tip. E_0 is evaluated accordingly to eq. 1.14 in the Tomlinson model. this formula implies F_L^{max}, the maximum lateral force in cross-sections through two-dimensional friction maps; like those in figures 3.4a, 3.5a, 3.6a.

3.3.5 Estimating the stiffness of the contact

For values of $\eta \gg 1$, the slope of the friction profile at the beginning of each sticking phase (k_{slope}) is considered in the literature to approximate well the stiffness of the system [92]. Carpick et al. performed measurements of the lateral stiffness of the contact between a silicon nitride cantilever and a muscovite mica in humid atmosphere. The sticking part of the friction loop was considered close to the value of the contact stiffness:

$$\frac{dF_{lateral}}{dx} = k_{eff} = \left[\frac{1}{k_{lever}} + \frac{1}{k_{contact}} + \frac{1}{k_{tip}}\right]^{-1}, \tag{3.4}$$

where $F_{lateral}$ is the lateral force (cantilever torsion), and x is the lateral displacement (see fig. 1.4). Typical lateral stiffness of commercial FFM cantilevers, k_{lever}, is around 50-100 N/m, at least one order of magnitude larger than the lateral contact stiffness, $k_{contact}$. The stiffness of the tip, k_{tip}, depends on the geometrical dimensions of the tip, and has typical values of tens of N/m. So, typical variation of the lateral force with x can accurately measure variations in the lateral stiffness of nanometer-sized contacts. Some corrections should be done for cases close to the transition point. Equation 3.2 presented in section 3.2 estimates real effective stiffness of tip-sample contact in conditions of η approaching 1. But for this values of k_{slope} and η are required. k_{slope} is accessible from friction measurements and η can be calculated with eq. 3.3 within the Tomlinson model. Knowing already F_L^{max} (or E_0) we can evaluate the dependence of η on normal

load F_N, fig. 3.10. Indeed, for small normal loads η approaches 1 within the errors bars.

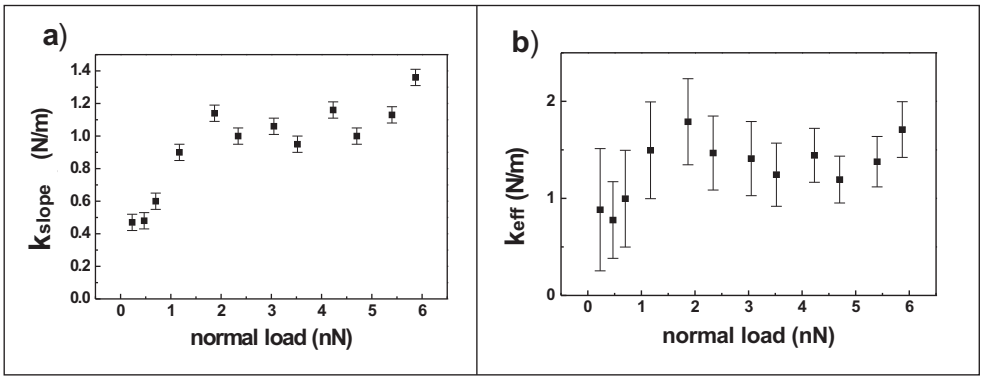

Figure 3.9: a) Slope k_{slope} of the experimental lateral force versus distance in the sticking part and b) effective lateral stiffness k_{eff} of the contact as function of the normal load F_N acting on the tip. k_{eff} is evaluated accordingly to eq. 3.2 in the Tomlinson model.

In figure 3.9 the evolution of k_{slope} and k_{eff} with F_N is presented. The small variation of the effective stiffness with normal load is less easy to understand. First let us note that the effective stiffness is of the order of 1 N/m, a range we have found in most of our atomic friction studies on different materials like NaCl(100), Cu(111), Cu(100) [73]. The cantilever and the deformable contact can be seen as springs in series (fig. 1.2 in section 1.3). The torsional stiffness of the force sensor is usually at least a factor of 50 higher. Therefore, the effective stiffness is clearly dominated by the contact which is a much weaker spring. For the occurrence of stick-slip processes in atomic friction, the stiffness of the cantilever-type force sensor does not play any significant role, as confirmed experimentally. The reason for the constancy of the contact stiffness could be explained in a straightforward manner by assuming that the atomic structure of the contact does not change in this range of normal loads. In this case, the deformability of the structure at the tip apex and of the surface around the contact would not change significantly with load. If the size or the atomic structure of the contact would change with load, the scaling of the corrugation and the stiffness would depend strongly on the dimensionality and commensurability of the contact [51]. Negligible friction between two solid surfaces is predicted when the interfacial interactions are weak or the surfaces are incommensurate [80].

The transition from stick-slip to continuous sliding observed for atomically modulated friction is then demonstrated experimentally and theoretically described. When the stick-slip instabilities cease to exist, a new regime of ultra-low friction is experienced. Negative and positive lateral forces sum up to a vanishing average force in the time average instead of the spatial average, provided there

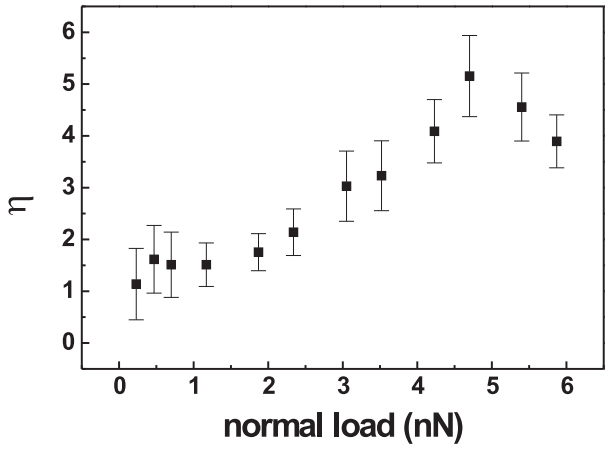

Figure 3.10: Parameter η calculated accordingly to eq. 3.3 as function of the normal load F_N acting on the tip.

are no instabilities. In our interpretation, no assumptions for a large contact size, hardness of the lattices, or commensurability have to be made.

We refrain to compare our results with the state of zero friction called by Hirano *superlubricity*, and related in his studies to an incommensurate contact between tip and surface [42]. This term could suggest that the transition to zero friction can be compared to superfluidity or superconductivity. However, this is certainly not an effect of quantum mechanical coherence. Furthermore, we assume that the mean friction is not zero, although we cannot measure any lateral force with the current signal-to noise ratio. The movement of the tip must be heavily damped, as we do not observe any overshooting or jumps over two lattice constants under stick-slip conditions. Consequently, there must be some energy loss mechanism in the tip movement beyond the internal damping of the force sensor. There is no reason to assume that this energy mechanism disappears for $\eta \leq 1$. What disappears, however, are the instabilities which under stick-slip conditions account for the by far dominating contribution to the observed dissipation. The damping in the force sensor and viscous movement of the sliding contact are certainly present and cause dissipation. These effects, however, are too small to be detected and are orders of magnitude smaller than the dissipation caused by a jump to a favorable energetic configuration.

It is important to note that a similar transition from stick-slip to continuous sliding has been observed in the manipulation of single Pb atoms by means of a scanning tunneling microscope [93]. In their study, Bartels et al. found a stick-slip process when the tip was moving relatively far from the Pb atom, while continuous sliding was observed with the tip in close proximity to the atom. The situation can be described in the same model as our experiment, but with the opposite tendencies. In the atom manipulation experiment, the surface corruga-

tion felt by the Pb atoms is always the same. When the tip was approached, the effective spring constant of the coupling between tip and atoms became higher, and therefore the stick-slip disappeared.

3.3.6 Influence of the tip "shape"

The experiment was repeated several times. Similar features were revealed with other tips on different spots of the crystal surface. The tips were never crashed or operated at high loads. In all cases the quality of the signal-to-noise ratio is reduced after prolonged scanning, making it difficult to recognize the transition from the stick-slip regime to continuous sliding.

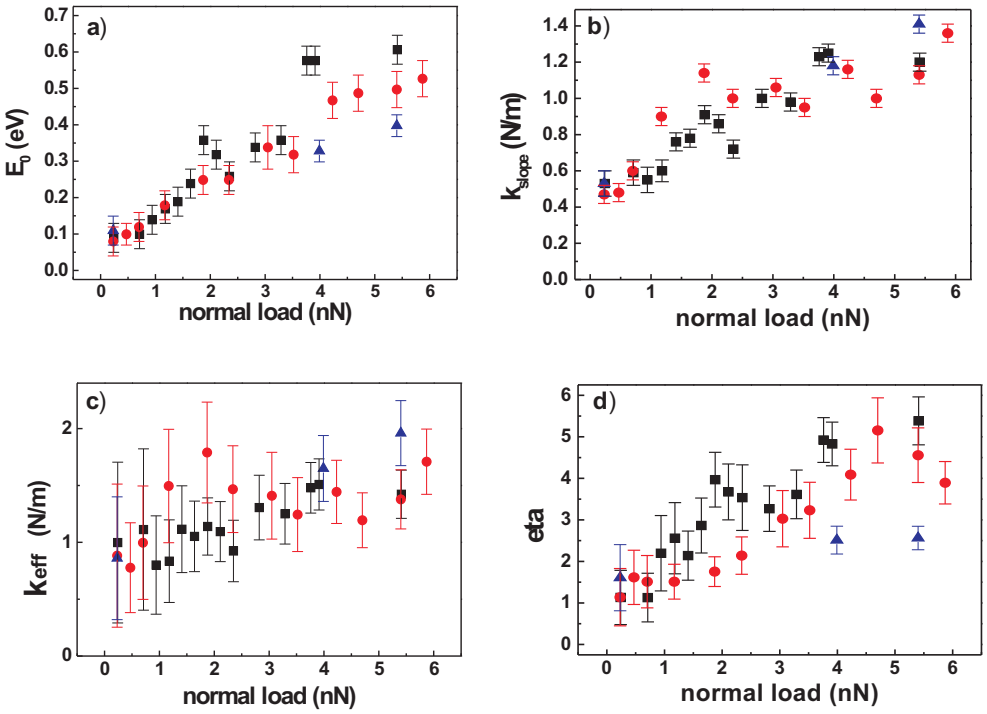

Figure 3.11: E_0, k_{slope}, parameter η and k_{eff} as function of the normal load F_N acting on the tip.

Fig. 3.11 presents the parameters E_0, k_{slope}, η and k_{eff} for three sets of measurements performed with the same tip on the same NaCl(001) surface. The results of the first set of measurements are marked in red, for the second in blue, and for the last measurements in black. For all cases, the four parameters show almost the same dependence on the normal force. The corrugation of the surface E_0 and implicitly, parameter η experience slightly higher values for the last measurements compared to the first, that can be explained through an increased

tip-surface contact area. This assumption is also sustained by a larger adhesion force recorded after prolonged scanning, 1.4 nN, whereas in the beginning the measured adhesion was only 0.7 nN.

3.4 Conclusion

Exploiting the high mechanical stability, and the optimized signal-to-noise ratio we were able to measure very small forces with very high resolution. We are able to control and reduce the applied normal forces down to 0.1 nN. These optimized conditions lead to the results presented in this section. We have experimentally demonstrated and theoretically described a state of ultra-low dissipation in atomic friction which is connected to the absence of mechanical instabilities. We observed the transition from a dissipative regime characterized by stick-slip motion to an ultra-low friction regime, when the tip slides continuously over the underlying surface. The transition can be controlled by variation of the load on the contact, which changes the atomic corrugation felt by the contact more than its stiffness. The results demonstrate how friction can be controlled on the nanometer scale and how stiff contacts with a binding in the contact that causes a weak potential against lateral sliding can practically decrease the dissipation. Based on experimental observations, it is assumed that the slipping movement of the tip is very strongly damped. It will be important for a full understanding of atomic friction experiments, and for the extension of the all friction results to understand and to explain the damping of the tip movement too. Recently, the dissipative coupling of the tip movement to phonons may be mediated by soft phonon modes that are induced by the presence of the tip [94]. Even more, it has been proposed that the dissipation occurs mainly inside the moving tip rather than in the sample; probable true, taking into account that the nanoscale tip is softer than the extended sample surface [95]. In reality, the detection of the all dissipation mechanisms and the determination of the precise place they occur implies highly sensitive experimental techniques, much more sensitive than the conventional scanning probe microscopy, and why not, even a completely different technique.

Nowadays nanotechnologists are aware that frictional forces become more and more relevant as the scale of a device is reduced [96]. Our results show that friction experienced on a *nanoasperity* is drastically reduced and even suppressed if the applied load is below a certain threshold. The strong point of this work is that we observe the ultra-low friction state without lubricants. This observation is a promising result for the practical realization of nanoelectromechanical systems (NEMS). In general, the output of an electromechanical device is the movement of the mechanical element [97]. Towards the shrinking tendency of the dimension of NEMS, the device physics becomes increasingly dominated by the

surfaces. Despite the increased ratio between surface and volume forces in these devices, an appropriate design of the sliding components should result in smooth motion with minimum energy consumption and without wear of the surface in contact. Three possible ways in achieving this objective can be thus suggested: i) To work at exceptionally low loads, as we did in our experiment or ii) to exploit the incommensurability between surfaces, as shown in the case of graphite [44], iii) or to excite the tip-sample contact at its resonant frequency [98]. The latter manner of reducing friction seems to be also a promising step forward controlling friction down to atomic scale and with practical applications in NEMS operation. Modification of friction forces by exciting the tip-sample contact in cases of normal oscillation of the cantilever or modulated applied bias voltage is the subject of chapter 4.

Chapter 4

Controlling atomic friction by applying modulated bias voltages

4.1 Introduction

Another contact AFM operating mode is the force modulation microscopy (FMM). In force modulation mode, the cantilever is caused to oscillate while the tip remains in contact with the sample surface. This may be achieved by applying a driving frequency to either the sample or the cantilever holder. As the tip position oscillates, the interaction force and hence the cantilever deflection changes. The sharpness of the change in deflection with position is related to the mechanical properties of the sample surface and the cantilever. In principle, it enables access to information about surface mechanical properties, because stiff materials should give rise to a sharper change in deflection with distance than soft ones. The FMM technique was pioneered by Veeco Instruments in 1989 [99], and enabled studies of relative difference in surface elasticity with high resolution for two different materials, carbon fiber and epoxy composite. The modulation frequency was in the range of kHz. This method is suitable for surfaces with soft and hard regions. In the literature there are many studies demonstrating the coupling between the normal and transverse motions in frictional sliding. Heuberger et

al. found that inducing normal (out-of-plane) vibrations between two boundary-lubricated sliding surfaces, load and frequency dependent transitions between a number of "dynamic friction" states could be observed. In particular, regimes of vanishingly small friction were obtained at interfacial oscillation amplitudes below 1 Å [56].

Artificially induced vibrations, both parallel and normal to the sliding direction, have long been used to reduce frictional energy dissipation in machinery [100, 101] and a number of simple models [102] are available for describing the transverse response to various types of dynamic modulations of the load. In all these models, the idea is that over some fraction of the oscillation the surfaces separate from contact and that during this period the friction is zero. This mechanism requires large driving amplitudes, sufficient to separate the surfaces even when they are in contact under a compressive load.

The following two sections 4.2 and 4.3 describe how an ultra-low regime of friction or even zero energy dissipated can be achieved in atomic scale friction by introducing a perturbation normal to the plane of sliding, like 1) normal excitation of the cantilever or 2) modulated bias voltage between tip and sample. During the sliding process the tip and sample remain in contact. The effect was observed for a wide range of normal forces, even for normal loads exceeding the threshold required to reach the transition to $\eta \leq 1$, as observed in the static mode presented in ch. 3.

4.2 Lateral force and normal force modulation on KBr(001)

Silicon cantilevers with a spring constant of $k_N = 0.03$ N/m for normal bending and $k_T = 18.06$ N/m for torsion were used. The radius of curvature of the tip was nominally below 15 nm (section 2.2). The feedback loop controlling the tip-sample distance was operated very slowly, in order to avoid any influence of the feedback on the measurement of the lateral forces. The experiments were performed on KBr single crystals cleaved in air, quickly introduced in UHV chamber, then heated at 150° C to remove charges produced in the cleaving process.

Fig 4.1 shows two 2D images: the lateral force in the forward scan and the frequency used to excite the piezo mounted on the back side of the cantilever. The normal excitation of the cantilever was continuously swept between 37-42 kHz. One-dimensional scans of 50 nm were performed with a scanning speed of 25 nm/s and an applied normal force of 0.17 nN. The cross section trough the frictional map indicates that the lateral force decreases for well determined frequencies. Calculating the average friction force for the 2D-image presented in fig. 4.1 we found out that the major decrease of friction takes place for f=40.25

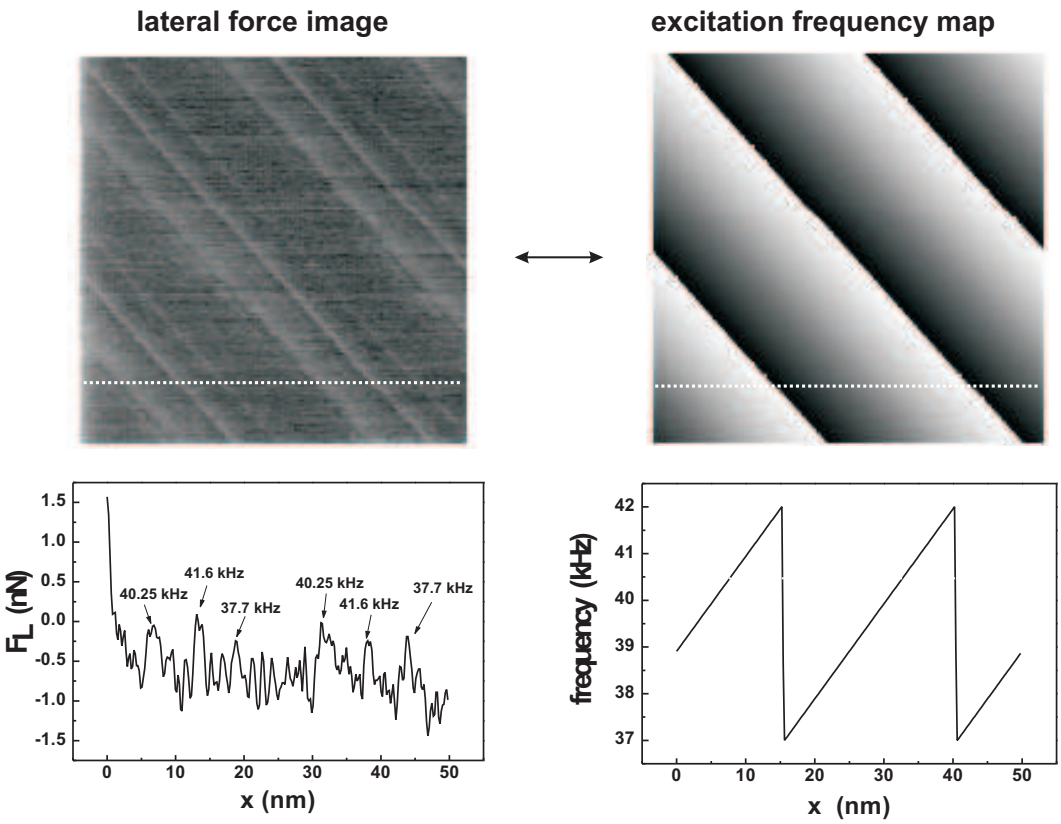

Figure 4.1: The lateral force image and the map of the continuous repetition of the swept normal excitation frequency (37-42 kHz). Below each image there is a cross section profile showing the simultaneous evolution of the F_L and the frequency.

kHz. In order to understand the origin of this frequency we measured the thermal noise spectrum of this cantilever in contact with the sample. Fig. 4.2a presents the thermal noise spectrum of the normal oscillation of the cantilever in contact with the KBr surface. In the range 0-200 kHz, the spectrum shows two peaks around 40.6 kHz and 126.4 kHz. The peak at 40.6 kHz is the first normal mode of resonance of the cantilever in contact, which is about five times higher than the normal resonance of the free cantilever (7.98 kHz). The second peak at 126.4 kHz is a higher harmonic of the normal oscillating mode. The resonance frequencies for different vibration modes for the free end cantilever and for the pinned end were calculated theoretically by Rabe et al. [103]. For a homogeneous beam of uniform cross section, the equation of motion for flexural vibrations is a differential equation of fourth order:

$$EI\frac{d^4y}{dx^4} + \rho wt\frac{d^2y}{dx^2} = 0, \tag{4.1}$$

where E is the modulus of elasticity, ρ is the mass density, and I is the moment of inertia. W and t are the width and the thickness of the cantilever, respectively.

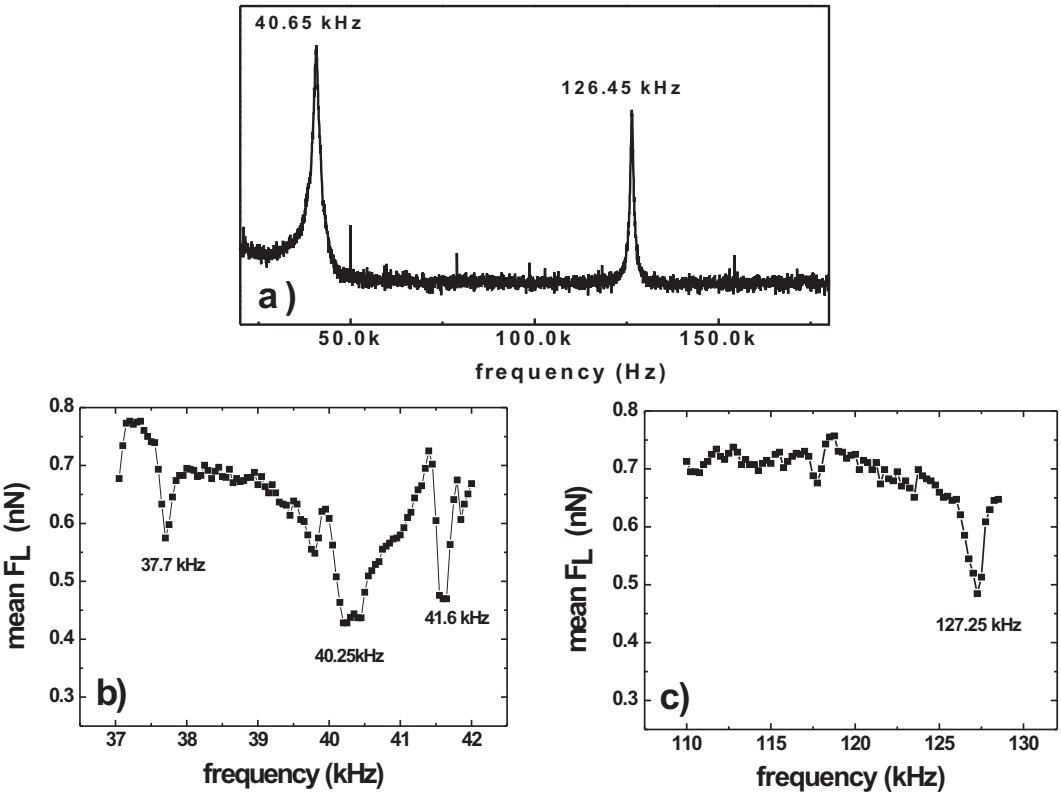

Figure 4.2: a) Thermal noise spectrum of the normal oscillations of the cantilever in contact with the surface. b) Frictional force while sweeping the frequency of the normal oscillation of the cantilever in contact in the range of 37-42 kHz. c) Frictional force while sweeping the frequency of the normal oscillation of the cantilever in contact in the range of 110-128 kHz.

For the cantilever clamped at one end and free at the other end (at $x = L$) the characteristic equation is:

$$cos(k_n L)cosh(k_n L) + 1 = 0, \tag{4.2}$$

where k_n is the wave number of the corresponding vibration mode and L is the length of the cantilever. The resonance frequency f_n belonging to k_n can be thus calculated:

$$f_n = \frac{(k_n L)^2}{c^2}, \tag{4.3}$$

where $c = L\sqrt{2\pi}\sqrt[4]{\rho wt/EI}$ is a constant containing the geometrical dimensions, Young's modulus, and the mass density. Solving numerically the equation 4.2,

it can be found the solution k_1L =1.875 for the lowest flexural vibration mode and the corresponding resonance frequency $f_1 = 1.875^2/(2\pi L^2)\sqrt{Ew^2/12\rho}$. The characteristic parameters of the silicon cantilever used in our experiment (L=450 μm, w=45 μm, t=1.16 μm, and ρ=2330 Kg/m^3, E=1.69·10^{11} N/m^2) led to a theoretical resonance frequency of the fundamental mode of 7.88 kHz, which is similar to the experimental observed frequency 7.98 kHz.

The resonance frequency of every mode of the clamped-pinned cantilever (when the spring constant of the contact between tip and sample becomes infinitely much higher than the spring constant of the cantilever) can be calculated solving the equation $sinh(k_nL)cos(k_nL) - sin(k_nL)cosh(k_nL) = 0$. The solutions of this eq. lead to resonance frequencies of the clamped-pinned mode higher that in the case of clamped-free cantilever. In accordance with theory, the frequency of the first pinned mode is 34.55 kHz, almost 4.5 times higher than the theoretical resonance frequency of the fundamental mode of the free end cantilever, but very close to the experimentally observed one, 40.6 kHz (see fig. 4.2a). The next pinned mode is found theoretically to be almost three times bigger than the previous mode, such that the peak observed in fig. 4.2a at 126.4 kHz is the second pinned vibrational mode.

Fig. 4.2b and c display the mean lateral force while scanning the KBr surface with a normally excited cantilever. The excitation frequency was swept around the first two resonance peaks of the tip coupled with the surface. When sweeping the frequency between 37 and 42 kHz, the friction force is reduced exactly for f=40.25 kHz. This frequency can be identified to be the first normal resonance of the tip in contact, 40.6 kHz. The two side peaks (37.7 kHz and 41.6 kHz) for which friction also decreases could be interpreted as satellites around the main resonance frequency. They might appear due to the continuous change in the contact between tiny asperities of the tip apex and the sample. In the range of 110-128 kHz, F_L decreases again when the external excitation matches $\sim$ 126.4 kHz, the second normal resonance.

Acoustic waves applied on the tip-sample interface showed distinguished influence of the in-plane and vertical surface oscillation components on the friction force experienced by a LFM tip in contact with the surface. Behme et al. studied the wave amplitude dependence of the friction. They proved that under the vertical component of the acoustic wave the friction force can be reduced and above a certain amplitude threshold, friction falls below the sensitivity of their instrument [104]. The effect was valid for a large variety of surfaces and for frequencies ranging from 200 MHz to 3 GHz. In the regime where friction within a standing wave field was completely suppressed, low frequency vertical cantilever oscillations were observed, whereas torsional oscillations were not excited.

4.3 Decrease of friction obtained by the modulation of bias voltages

The suppression of friction can be also obtained by producing a localized perturbation at the tip-sample contact if an *ac* bias voltage is applied. Our experiment was realized on two insulating materials, KBr and mica, cleaved in air and then quickly introduced in UHV. The thickness of KBr was 1.23 mm, and 0.2 mm for mica. Measurements on KBr were performed with a silicon cantilever having a spring constant of $k_N = 0.03$ N/m for normal bending and $k_T = 18.06$ N/m for torsion, whereas on mica the cantilever characteristics were $k_N = 0.05$ N/m and $k_T = 27.84$ N/m. Fig. 4.3a shows the average friction force measured when an *ac* bias voltage with an amplitude U_B=8V and frequencies in the range 0-300 kHz was applied between the silicon tip and the insulating KBr surface. The dependence of F_L on the modulation frequency of U_B was obtained scanning three regions of 100×100 nm^2 each, with a scan speed of 100nm/s and a normal force F_N= 3.9 nN , while the frequency was swept between 0-100 kHz, 100-200 kHz, and 200-300 kHz, respectively. As one image consists of 256 lines, the time necessary to acquire it was 512 s. The sampling rate for sweeping the frequency has been chosen to be 200 Hz/s, such that during one scan (512 s) a range of 100 kHz could be swept (500 s). Part b) of the same figure shows the resonance peaks of the cantilever in contact with the KBr surface. The peak at 40.8 kHz corresponds to the first normal mode of the cantilever in contact with KBr, and the following peaks at 126.9 and 260.4 kHz are the resonances of the second and, respectively, third normal vibrational mode of the tip-sample system. The peak marked in red at 174.4 kHz is the first torsional resonance of the cantilever in contact. For common rectangular AFM cantilevers, the resonance frequencies of the torsional modes are much higher than the resonance frequencies of the 1st normal vibrations. The equation of torsional motion is a differential equation of second order [105]:

$$C\frac{d^2\theta}{dx^2} = \rho J\frac{d^2\theta}{dx^2}, \tag{4.4}$$

where θ is the angle of torsion of the cross-section area, C is the torsional stiffness, ρ is the mass density, and J is the polar area moment of inertia. If the cross section is rectangular, the polar moment of inertia and the torsional stiffness are given by: $J \approx w^3t/12$ and C= $wt^3G/3$, where G is the shear modulus of cantilever. Since the differential equation for torsional vibrations is only of second order, the phase velocity v is a constant $v=\lambda f=\sqrt{C/\rho J}= 2t/w\sqrt{G/\rho}$ and the modes are equidistant in frequency:

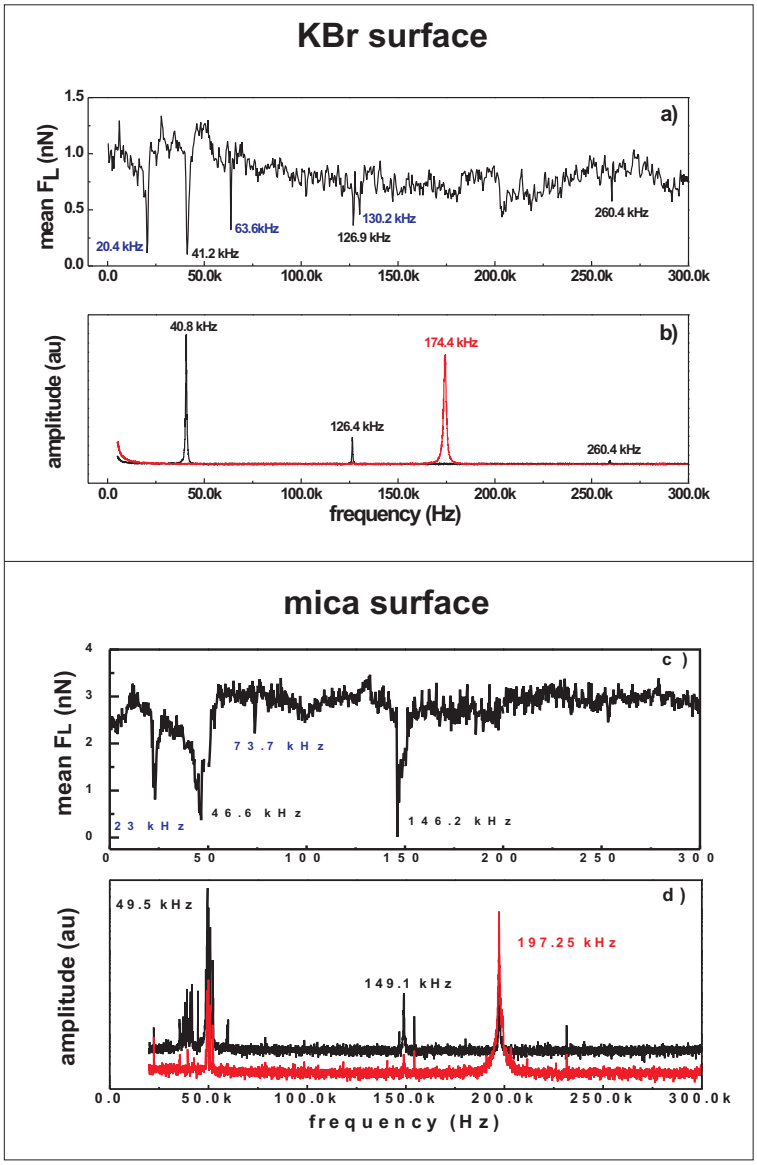

Figure 4.3: Average value of the friction force on a) KBr and c) mica surface acquired while applying modulated bias voltage with frequencies between 0 and 300 kHz. The peaks marked with blue appear due to the non-linearity of the oscillatory system and they are exactly half of the resonance values. Thermal noise spectrum of the normal (black line) and torsional (red line) oscillations of the cantilever in contact with the b) KBr and d) mica surface. Note that for these two sets of measurements two different tips were used. The tip scanned on KBr showed a first resonance of the free cantilever at 7.98 kHz, and for that used on mica, f_0=9.2 kHz.

$$f_T^n = \frac{2n-1}{2L}\frac{t}{w}\sqrt{\frac{G}{\rho}}. \tag{4.5}$$

The lowest torsional vibration frequencies are about ten times higher than the flexural frequencies for typical AFM cantilevers. Using eq. 4.5 and the characteristics of the cantilever (L=450 μm, w=45 μm, t=1.16 μm, and ρ=2330 Kg/m^3, G=0.5·10^{11} N/m^2) a theoretical torsional resonance of the free end cantilever can be calculated f_T^0=132.68 kHz, similar to the experimental value 149.9 kHz. If the end of the cantilever is not free, but pinned, the resonance frequency is shifted almost 20% to upper frequencies [106]. Therefore, the peak at 174.4 kHz is in our case the first mode torsional resonance of the cantilever in contact with the KBr surface.

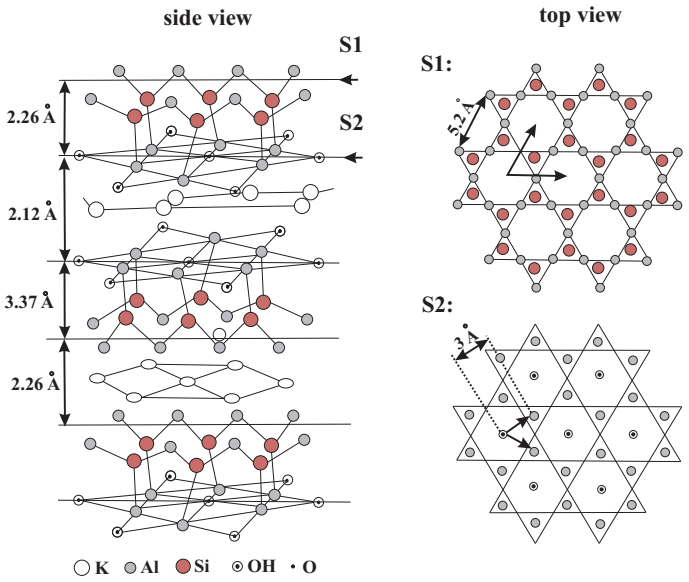

Figure 4.4: Crystallographic structure of mica. Top view of the layer S_1 shows the array of hexagonal rings formed by the bases of SiO_4 tetrahedra. Top view of layer S_2 below the SiO_3 bilayer. The sites are occupied by O and OH groups with a periodicity of 3.0 Å, and form an angle of 30° with the former lattice direction. The K^+ ions on top of the S_1 layer are not shown [59].

The experiment on KBr was repeated on mica, a completely different surface. The atomic structure of mica is not as simple as in the case of KBr. Because of this particular atomic arrangement (see fig. 4.4), the physical properties exhibit a rather strong anisotropic behavior, and the frictional forces depend on the scanning direction [107]. Despite these differences, the effect on friction of the modulated bias voltage between tip and mica sample is the same as for KBr. Fig. 4.3c shows how the mean lateral force drastically decreases when the applied ac

bias is modulated *only* with the normal resonances of the cantilever in contact with the surface. It is interesting to observe that friction tends to zero also when U_B is modulated at *half* the values of the normal resonance frequencies, those marked with blue in figures 4.3a and c. *No effect was revealed at the torsional resonance.* For the measurements on mica a cantilever with the first flexural resonance at 9.2 kHz was used. Consequently, in fig. 4.3d all the resonance peaks are shifted to higher frequencies, compared to those obtained with the previous tip on KBr. The third flexural mode around 260 kHz does not appear in the power spectrum measured on mica. Probably, due to specific coupling between the silicon tip and mica surface this mode of vibrating has a quality factor too low to be detectable.

In order to understand whether the averaged friction force suffers only a reduction or it can reach negligible values, comparable to those described in chapter 3, we swept the excitation frequency with lower speeds. Fig. 4.5 answers this question showing the value of F_L obtained while sweeping the same range of frequency 37-44 kHz with two rates: 200 kHz/s in fig. 4.5a and, respectively, 14 kHz/s in the part b of the same figure. Indeed, for excitation frequencies correspoding to the normal resonance frequencies *friction goes down to zero.*

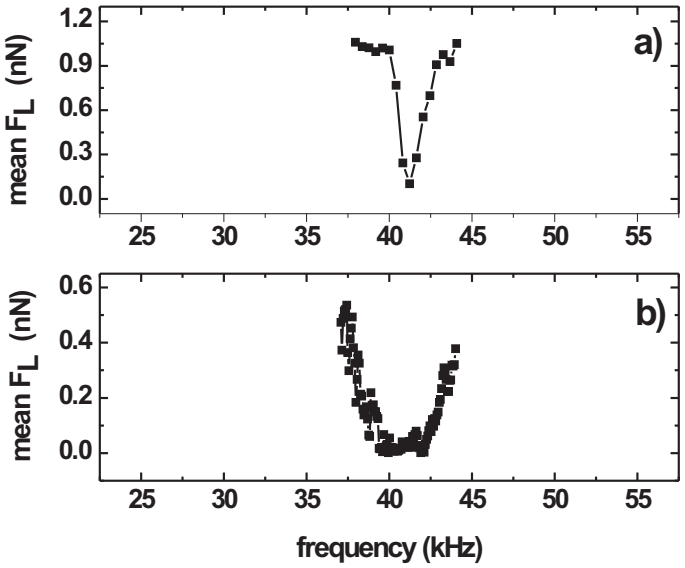

Figure 4.5: a) Friction force recorded while sweeping the frequency with a rate of 200 Hz/s. b) F_L was recorded with a lower sampling rate (14 Hz/s). Friction goes to zero when the frequency matches perfectly the normal resonance of the couple tip-sample system.

In order to explain our results, we have to compare the two types of perturbation induced at the tip-sample interface: (*i*) direct normal excitation of the cantilever in contact, and (*ii*) applied modulated bias voltage. Both procedures

led to the same effect: reduction of friction only for normal resonances of the tip in contact with the surface. Under resonance conditions the instantaneous normal force acting on the tip is continuously oscillating. The feedback loop can not follow the fast variations of this force, but just tries to keep constant the mean value of the normal force, chosen as setpoint for the measurements. At low enough normal loads, the motion of a sharp tip sliding on a crystal surface is determined by the local interactions and by the combined elastic deformations of the materials in contact [35]. The elastic deformation is represented in 2D by a parabola of curvature k_{eff} equal to the effective lateral stiffness. The interaction between tip and sample can be described by a potential having the spatial periodicity of the crystal and lateral corrugation $E_0(F_N)$ increasing with normal load [108]. Introducing the parameter $\eta = 2\pi^2 E_0/K_{eff}a^2$, where a is the lattice constant of the crystal, the condition for disappearance of stick-slip is η <1, see paragraph 3.2.

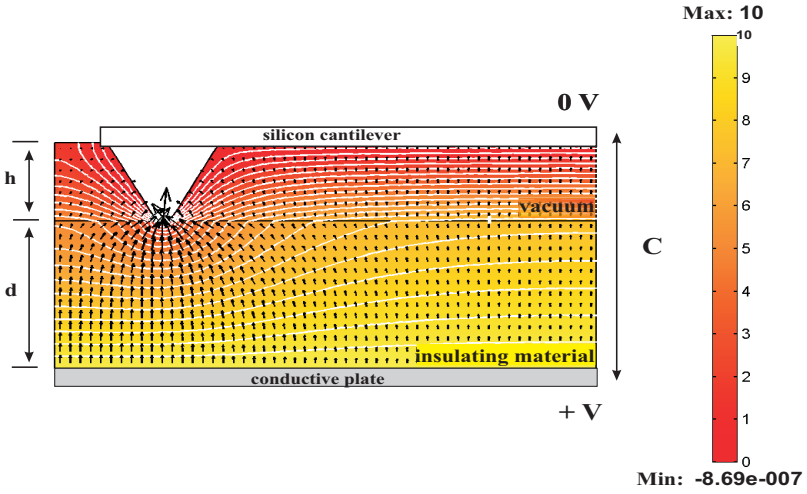

Figure 4.6: Sketch of the electrostatic field between the cantilever and the conductive plate behind the sample. The cantilever and the sample can be seen as a capacitive system (d ≫h), where the insulating KBr or mica are the dielectric media separating the conductive parts of the capacitor.

If the *ac* voltage is switched on, the ionic crystal can play the role of a dielectric medium placed between two conductors. Because the thickness of the sample is much larger than the tip height (d=1.23 mm and h=12 μm), the capacitive interaction occurs mainly between the cantilever body and the sample holder. This interaction results in a capacitive force, F_U, proportional to the square of

the applied voltage. The attractive force F_U oscillates with *twice* the excitation frequency *f*. Besides F_U, any charge trapped at the tip or any charge layer at the surface results in a non-zero contact potential and in an additional force F_Q, which oscillates at the actuation frequency *f* [109]. An attempt for the estimation of the capacitive force can be done considering that the effective area of the capacitive system is given by the dimensions of the cantilever, S=L·w. The counter electrode is considered to be an infinite plane with uniform charge distribution, σ. Note that the force applied strictly on the tip prevails only for small distances, d <100 nm, while for large distances the cantilever gives the main contribution to the force [110]. The field created by this is E=$\sigma/(2\epsilon_0\epsilon_r)$, where ϵ is the permittivity of dielectric medium. The force developed by the electric field on the cantilever, assuming that the charge is also uniform distributed all over the area S, is then:

$$F_U = \frac{\epsilon_0\epsilon_r}{2}E^2S = \frac{\epsilon_0\epsilon_r S U_B^2}{2d^2}, \tag{4.6}$$

where U_B is the amplitude of the modulated bias voltage. The electric field inside the capacitor is sketched in fig. 4.6, and it can be seen that it acts all along the cantilever length. The electrostatic force produces an additional vertical displacement of cantilever, A_U, which is too small to produce a noticeable effect. Under resonance conditions A_U is amplified by the Q factor of the normal vibrations leading to a total displacement:

$$A_{res}(n) = QA_U = Q\frac{F_U}{k} = Q\frac{F_U}{m(2\pi f_n)^2} = Q\frac{\epsilon_0\epsilon_r S U_B^2}{2d^2 m(2\pi f_n)^2}, \tag{4.7}$$

m is the mass of the whole cantilever and f_n is the resonant frequency of the n-th flexural mode. The quality factors of any vibrating mode can be determined by an analysis of the amplitude spectrum of thermal noise of the cantilever. The spectral amplitude density is:

$$S(\omega) = \frac{2k_BT\omega_n^3}{Qk_n[(\omega^2-\omega_n^2)^2 + \omega_n^2\omega^2/Q^2]}, \tag{4.8}$$

where ω=$2\pi f$ is the radical frequency, and k_n is the string constant of n-th mode. The quality factor of the first three normal vibration modes (see fig. 4.3b) are presented in the table 4.1.

Using eq. 4.7 and the quality factors of the first three normal modes, the corresponding A_{res} for each oscillation mode can easily be estimated, as it can be seen in table 4.1. The obtained values can thus explain the dependence of frictional forces on the excitation frequency depicted in fig. 4.3b. The application of the ac bias voltage provokes a normal modulation of the cantilever with an amplitude proportional to the amplitude of U_B and strongly dependent on the properties of the flexural resonance.

The transition between a frictional sliding of two bodies in contact and a regime of zero friction force is a reversible process. Actually, friction can be

Cantilever in contact with KBr ϵ_r(KBr)=5.65			
n	1st normal mode	2nd normal mode	3rd normal mode
f_n (kHz)	40.653	126.395	259.389
Q	98	450	761
A_{res} (Å)	6.2	2.94	1.18

Table 4.1: The resonance frequency for the first three flexural vibration modes of a rectangular silicon cantilever in contact with a KBr sample, the corresponding quality factor and induced amplitude under resonance conditions, A_{res}.

turned *on* and *off* by exciting the cantilever at an appropriate frequency. Fig. 4.7 presents a friction loop recorded over 5 nm with a normal force of 0.67 nN. A bias voltage with an amplitude of 5V and modulated with $f = 41$ kHz applied after scanning 2 nm, led to the suppression of the loop even under the action of a relative high normal load. The corresponding parameter η for this load is around 3.8, meaning that the sliding should occur under static conditions with dissipation. In the presence of U_B the tip started to move without friction, still maintaining a contact with the KBr surface. Scanning back, the bias voltage was switched off at the same scanning position where it was applied and the friction loop came back to the initial shape.

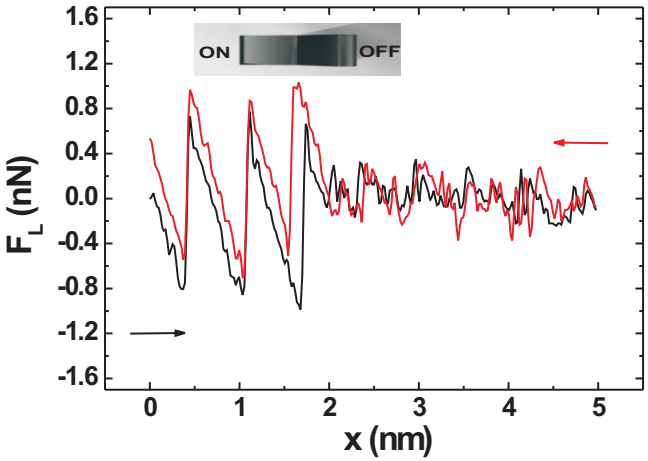

Figure 4.7: Friction loop on KBr obtained with a normal load F_N=0.67 nN. At the moment when the loop shrinks or extends a bias voltage with f=41 kHz and amplitude of 5 V was applied and, respectively, removed.

In other words, the bias voltage applied in the conditions just mentioned above plays the role of a "switch", which turns on and off a state of superlubricated sliding. By applying U_B under resonant conditions, the common stick-slip observed

in atomic friction can be suppressed. The less corrugated surface potential, for almost half of the actuation period, leads to a reduction of the energy required to move the tip from one minimum to the next one. As described in chapter 3, if the surface potential is sufficiently small the tip can slide over the surface with negligible friction. An opposite direction of deflection would lead to an increase of the surface corrugation potential, thus to enhanced friction. The change in sign for the amplitude defection takes place in half of the oscillation period (t=1/2f= 12.29 μs), a too short time for the contact spring to get the necessary strength for a new jump (the time constant of sticking phase is around 100 ms). In this condition the stick-slip motion is not favorable and the tip will move all the time on a smoothly corrugated surface potential, such that its sliding takes place without dissipation.

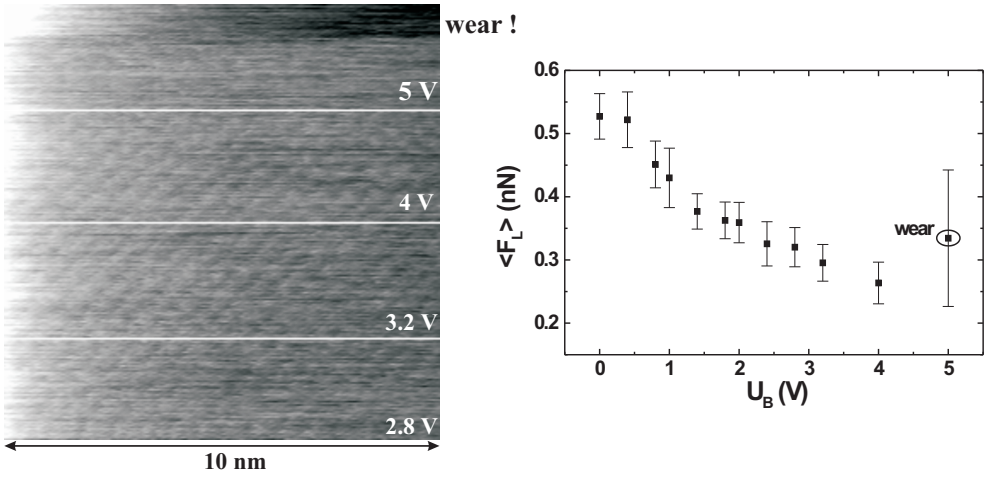

Figure 4.8: 2D map of the lateral force for four different amplitudes of U_B. Wear process is initiated when U_B reaches 5V. Friction force versus the amplitude of the applied bias voltage modulated with f=39.9 kHz. The mean normal force was 0.03 nN. Measurements were done on a 2-nd KBr sample, much thinner than the first one (d=0.83 mm).

Fig. 4.8 presents the influence of the bias voltage amplitude on the recorded friction force. We kept the modulation frequency constant, close to the first normal resonance (f= 39.9 kHz) and performed measurements for U_B between 0 to 5 V. The thickness of the KBr sample under observation was thinner, d= 0.83 mm. A decrease of the the mean lateral force with U_B was observed, a result that can be explained by the dependence of the induced oscillation of the cantilever on the amplitude of the applied bias voltage. The larger the induced deflection of the cantilever, the larger the effect of reducing friction. If A_{res} is very large, then the cantilever deflections toward the sample lead to a tip-sample interaction strong enough to initiate wear. This is what happened for U_B = 5 V, when after

few scanning lines the lateral force became irregular and the tip started to wear the surface. Large amplitudes of U_B leads thus to an interesting behavior, the coexistence of a regime of low-friction and wear. The last one dominates, short time after it was initiated. This phenomenon was already observed in macroscopic friction between two glass polymer materials, where relative large amplitude (20% of the mean normal load) led to a nonlinear coupling between normal and sliding motion, accompanied by a destabilizing effect in same regions of contact [55].

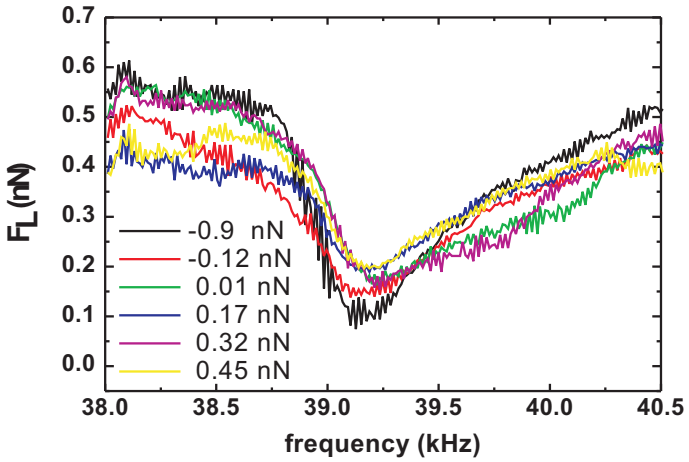

Figure 4.9: Mean lateral force while sweeping the frequency of U_B between 38-40.5 kHz. Measurements were performed for different values of the normal load. The thickness of the KBr sample was d=0.83 mm.

We have also studied the effect of the normal load acting on the cantilever. The influence of the setpoint while sweeping the frequency of the ac bias voltage with an amplitude of 3 V is presented in figure 4.9. For negative setpoints, when the tip-sample interaction is in the attractive regime, the effect of the bias on the friction force is larger than for positive normal forces, when the interaction is already in the repulsive regime. This could be easily explained in terms of tip-surface lateral corrugation variation. The effect of the normal modulation on the lateral tip motion can be understand by assuming that the corrugation energy changes with time as $E(t) = E_0(1 + \alpha cos 2\pi f t)$, where the parameter α is proportional to the amplitude of the applied voltage and exhibits maxima at the bending resonances. The forces acting on the tip balance at every instant, and all equations derived in the quasistatic case, $\alpha = 0$, such that $E(t)$ replaces E_0. Typically values for the stiffness of the tip apex is around 1 N/m (i.e., much lower than k_T). This finding strongly suggests that the tip apex is mainly responsible for the slips rather than the cantilever. In order to clarify the observed suppression of friction, the lateral deflection of the cantilever is ignored and the equation of motion of the tip apex connected by a spring of lateral stiffness k=1 N/m to

an essentially rigid object (the remainder of the tip plus the lever) pulled along the scan direction at a low velocity v=10 nm/s across an oscillating sinusoidal potential with spatial periodicity a=0.5 nm:

$$m\frac{d^2x}{dx^2} + \gamma\frac{dx}{dx} - \frac{\pi E_0}{a}(1 + \alpha sin2\pi ft)\sin\frac{2\pi x}{a} + k_{eff}(x - vt) = 0. \tag{4.9}$$

The mass and damping of the tip apex are difficult to determine. Because f is much smaller than the time needed for the tip to go over one atomic lattice, the tip experiences the minimum corrugation $E_0(1-\alpha)$ many times as the rigid tip slowly crosses the distance which separates adjacent potential minima, and hence stats to slide smoothly once:

$$\eta_{min} = \eta(1-\alpha) = 2\pi^2 E_0/(k_{eff}a^2) < 1, \tag{4.10}$$

even if friction is finite ($\eta > 1$) when $\alpha = 0$. In other words, the parameter η_{min} replaces η in the condition for the occurrence of "superlubricity". It is important to mention that for sufficient negative setpoints (already small η) and large bias voltages, the tip-sample separation becomes too large and the tip jumps out of contact.

As we have discussed, the parameter η can be tuned by decreasing the normal forces (implicitly decreasing the amplitude of the corrugation E_0) or by modulating this corrugation. In order to have a complete picture of the effect of E_0 modulation we performed friction measurements also on NaCl(100), a material less compliant than KBr, such that wear process can could be avoided. Friction between the silicon tip the NaCl(100) sample was recorded while exciting the tip in contact at the main normal resonance f_0= 56.7 kHz. In fig. 4.10a the effect of the modulation amplitude is shown. The mean friction force decreases with the increase of U_B. The modified Tomlinson model at 0 temperature described in section 3.2b can reproduced a similar curve for the dependence of the friction force on the amplitude of the modulation of the surface corrugation, α (see fig. 4.10b). In the simulation, it was considered that the only last part of the tip, is responsible for the reduced friction effect. By solving the equation of motion 4.9 for a tip apex of a mass m =8.7 10^{-13}, ten times critically damped γ/m= 126 kHz, oscillating at 567 Hz, the friction force decreases as the parameter α increases. Figure 4.10b shows this behavior for different values of η (values calculated in the static regime). Plotting the same forces, F_L against the parameter $\eta_{min} = \eta(1-\alpha)$, one can see that the friction force decreases and even goes to zero as soon as the eta_{min} approaches 1 or gets smaller than 1 (fig 4.10c). Depending on the values of η and $\alpha(eta_{min}) = \alpha_{cr}$ (the value ofα for which the F_L is suppressed), two sliding regimes are possible, as shown in the figure 4.10d.

For many years the control of frictional forces has been mainly approached by chemical means, namely, using lubricating liquids. The application of an *ac*

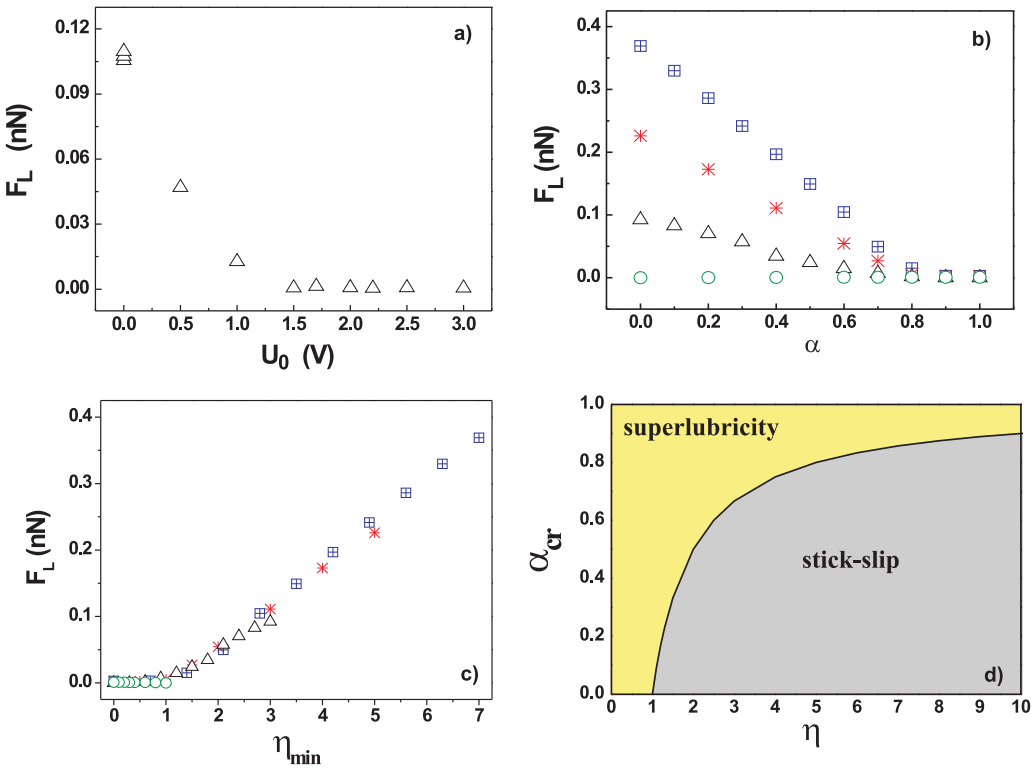

Figure 4.10: a) Dependence of the friction force on NaCl(100) on the amplitudes of the ac voltage at the resonance frequency f = 56.7 kHz. An average normal load FN = 2.73 nN was kept constant by a feedback loop (corresponding to $\eta = 3$ in the static case). b) Numerical evaluation of the frictional force as a function of the excitation amplitude. The four symbols correspond to $\eta = 7$, 5, 3 and 1 (top to bottom). c) Numerical values of the frictional force as a function of the parameter η_{min}. d)Depending on the values of η and $\alpha(\eta_{min})$, two sliding regimes are possible.

modulated bias at the right amplitude and frequency is equivalent to the presence of normal force oscillations between two bodies sliding in contact. The method of controlling the system mechanically via normal vibrations of small amplitude and energy is already a promising alternative to the traditional ways of modifying friction, and has attracted considerable interest recently. Gao et al. [54] proposed this method for controlling and reducing friction in thin-film boundary lubricated junctions, through coupling of small amplitude directional mechanical oscillations of the confining boundaries to the molecular degrees of freedom of the sheared interfacial lubricating fluid. They performed MD simulations proving that the

control of friction in the lubricated junction is possible, with a transition from a high-friction stick-slip shear dynamics of the lubricant to an ultra-low kinetic friction state, if the time constant of the boundary mechanical oscillations normal to the shear plane is larger than the characteristic relaxation time for molecular flow and ordering processes in the confined region. Thus, the decrease of the frictional force can be obtained by controlling the system mechanically.

Beside the friction dependence on the normal resonance frequencies there are studies emphasizing the same effect, but under the action of lateral (in-plane) oscillations. Rozman et al. [111] analyze a theoretical one-dimensional model including two rigid plates and a single particle embedded between them, in which the top plate is pulled by a linear spring with a force parallel to plane of sliding. The time dependence of the spring force drives from a chaotic motion to smooth sliding of the system. In contradiction with our findings, there are experimental proofs of atomic friction control via lateral induced oscillation. Kerssemakers at al. probed the influence of the in-plane vibrations on the shape of the surface potential involved in stick-slip friction [98]. Modulation of the cantilever was performed in two ways: either a high-frequency modulation (buckling mode) was summed on the piezo scanner voltage, or electrostatic loading was applied. These modulations diminished the friction loop amplitude, and furthermore, a partial stick-slip behavior was observed above a certain threshold level of driving amplitude, where the tip alternated periodically between a zero-friction and a non-zero-friction state.

A partial reduced friction has previously been achieved by exciting oscillations perpendicular to the sliding direction in different situations, e.g. force microscopy of transition-metal chalcogenides [112], wide contact areas subject to ultrasonic excitation [113], in the presence of confined lubricant films [56], or between glassy polymers [114]. In those investigations, however, the reduction of friction remained unexplained or it was attributed to an induced lateral motion of the tip [112], or to an increase in the mean separation between the two surfaces [113, 56].

Riedo et *al.* observed a partial reduction of friction when the contact between a conventional FFM tip and a mica surface in humid air was laterally excited at 20 kHz, in the low-velocity range where F_L is reduced by thermal activation [91]. They show that the atomic friction is related to the thermally activated hopping of the contact atoms on an effective atomic interaction potential. The thermally activated friction is responsible for the premature jumps of the contact from one minimum to the next minimum position of the total interaction potential and leads to a decreased energy dissipation in sliding. They claimed to identify the the hopping frequency with the lateral the lateral resonance of the system , 20 kHz, but the actual torsional resonance in contact was not measured in that experiment. In our case reduced friction is expected if the displacement of the tip induced by lateral excitation reaches roughly half a lattice constant. Taking into account that the quality factor decreases by a factor of at least one hundred

upon contact, it is perhaps not surprising that the stick-slip is maintained and that no significant reduction of friction was observed under torsional excitation.

4.4 Conclusion

We proposed an efficient way to switch friction on and off on the atomic scale is introduced. This is achieved by exciting the mechanical resonances of the sliding system perpendicular to the contact plane. The resulting variations of the interaction energy reduce friction below 10 pN in a finite range of excitation and load without any noticeable wear. Without actuation, atomic stick-slip leading to dissipation is observed in the same range. Even if the normal oscillations require energy to actuate, our technique represents a valuable way to minimize energy dissipation in nano-contacts. We verified this method on two different surfaces and we proved that this behavior is generally valid on different kind of material.

Controlling friction in nanoelectromechanical systems (NEMS) is not only a desirable goal, but a necessity to guarantee an extended lifetime of the devices themselves. The extension of our work to NEMS devices should be quite feasible. During sliding of NEMS components a modulated bias voltage with adequate amplitude and frequency can be applied, leading to a significat reduction of friction of such devices. It is important to mention that in these systems the ratio between surface and volume is extremely high. Contacting parts in NEMS are usually small enough to constitute single asperity contacts, and their structure favors the development of distinct normal resonances. In macroscopic bodies, the wide distribution of contact resonances makes our technique difficult to apply, but it is not excluded that resonance-induced superlubricity occurs in many natural phenomena, for example in biological systems or, on much larger scales, in the motion of tectonic plates.

Chapter 5

Wear on atomic scale

5.1 Introduction

"*But there are also situations when one wants high friction, as in clutches and brakes, or stick-slip, to enrich the sound of a violin and improve the feel or 'texture' of processed food as sensed during biting and chewing...*"

If the AFM is operated in contact mode, several regimes from frictionless sliding to permanent wear are observed, depending on the applied load. In this way, FFM has been successfully used to characterize microwear processes on materials of technological interest, as silicon for magnetic head sliders [115], polymers for electronic packaging and liquid crystals displays [116], or solid lubricants such as transition metal dichalcogenides [117]. Only a few studies have been reported on atomic-scale wear, mainly due to the fact that the debris removed from the surface adheres strongly to the tip, reducing the resolution of the instrument and making investigations non-reproducible. The environment, like the humidity, plays an important role in tribological measurements on small scales [21]. A controlled atmosphere or, better, ultrahigh vacuum (UHV) conditions are desirable.

Metals are not the best candidates to study wear mechanism by AFM. Previous experiments on copper and aluminium showed that the debris accumulates

on the microscope tip, making it blunt and not suitable for reproducible measurements [118]. In the case of ionic crystals wear is observed even at very low loads [57, 58]. If the normal force exceeds a critical value the process of wear is initiated. In fig. 5.1 the wear onset on atomic scale is illustrated. The sample involved is KBr(001), as ionic crystals are well know materials for their low reactivity and the measurements were performed in UHV. The atomic structure is obtained with a normal load acting on the tip of only 1.3 nN.

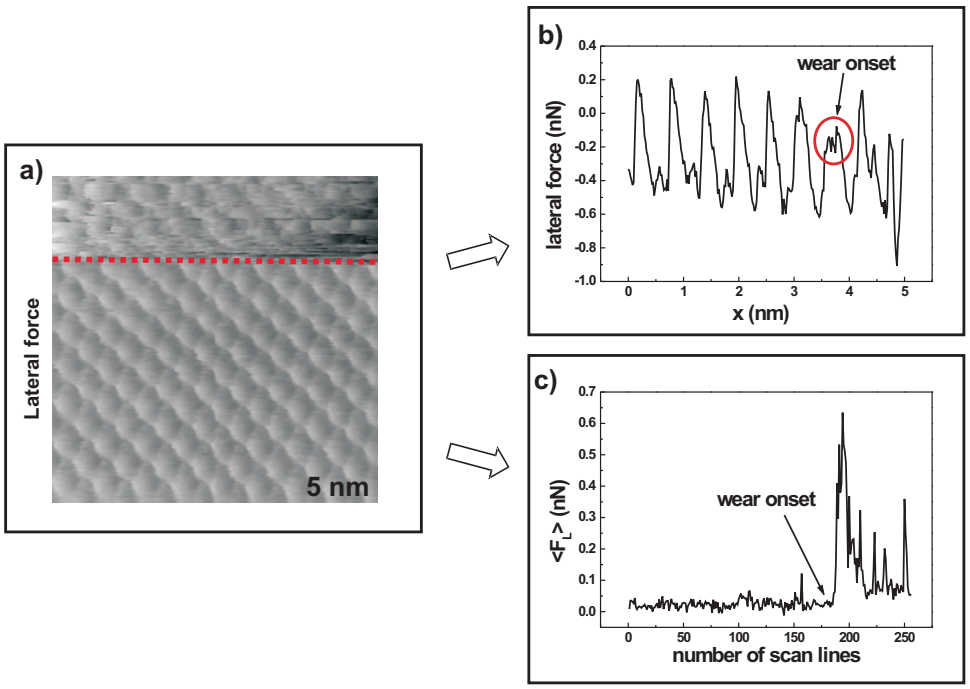

Figure 5.1: Lateral force measurement on KBr(001) in UHV with an external applied load of 1.31 nN. a) Friction map on 5 nm revealing the moment when the atomic structure starts to become irregular, due to the wear process. b)Cross section of the lateral force emphasizing the wear onset too. c) The mean lateral force over the 2-dimensional image. In the moment when the regular atomic structure is broken the abrasive wear starts.

In the initial part of the 2D image 5.1a the lateral force presents a regular behavior, as seen in the cross-section presented in the b) part of the figure too, it presents the well defined saw-tooth profile with atomic periodicity. But at a certain moment an instability occurred, the tip started to pick up material and the regularity of the stick-slip got broken. At this point the friction force was drastically increased initiating the wear process (part c)). The high value of F_L led to the detachment of atoms. This is the wear onset observed down to atomic scale. Immediately after this process got initiated, the lateral force becomes ran-

dom, and the surface suffered a continuous rearrangement as it could be seen in the 2D friction map (fig. 5.1a).

5.2 Abrasive wear on atomic scale

In order to understand how the wear process is initiated and how the material is transported by the tip, Gnecco et al. studied wear on ionic crystals by means of an AFM [58]. They showed how under the action of the tip the KBr(001) surface can be modified, the ions removed pairs by pair and dragged collectively by the indenter. Furthermore, the debris is rearranged in a epitaxial process leading to the formation of mound with the same structure as the underlying surface. The images of damaged areas were used to count up the number of atoms torn from the surface. Knowing the binding energy of atoms in the crystal, it was possible to calculate two separate contributions to scratching energy. According to this paper, 30 % of the energy goes into wear. The work shows new details of wear process and demonstrates a level of control that might be used for micromachining. We tried to go further on in studying wear on atomic scale and we performing one and two dimensional scratching measurements on a scale of hundreds of nanometer.

Extending the wear process in 2D, the formation of nanometer-scale patterns while scratching the KBr(001) surface with a scanning force microscope in ultra-high vacuum can be produced. Wear of single atomic layers has been observed when the microscope tip is repeatedly scanned across a line. The initially flat surface is rearranged in a quasiperiodic pattern of mounds and pits.

5.2.1 KBr "ideal" surface

All the experimental wear observations we got on KBr crystals and the necessary conditions for the initiation of this process have been previously confirmed by theoretical studies based on atomistic simulation of the interaction between a crystalline sample and a nanoasperity tip. Shluger at al. have analyzed two cases for the nanoasperity at the end of the tip: 1) a locally charge tip, MgOH, scanning over the (001)NaCl surface and 2)a neutral tip, MgO, interacting with the (001)LiF surface [119]. In each situation it has been demonstrated that the tip-sample interaction has a collective character: the tip as a whole probes the potential produced by the whole surface in the area of several surface ions averaged in time. In the case of MgOH tip while scanning with positive forces after the jump in contact (the attractive regime) a wide range of deformations, often reversible, of the tip and sample have been encountered. A continuous interchange of material between tip and sample was noticed. The ionic tip adsorbed ions from the ionic sample and used them for a while in subsequent scanning. During operation of the AFM, the tip almost certainly reaches some steady-state

dynamical balance of adsorbing and desorbing atoms by the time the image is acquired. The same behavior was observed for metallic tips interacting with metal surfaces [120, 121]. The inert sharp MgO tip showed the same sample periodicity while scanning in contact with small normal forces, as the charged tip. A shift of the position of the atoms relative to the surface sites depending on the tip orientation was observed.

The same theoretical study showed that in hard contact a positive bending of the cantilever counting for a total tip load of 2nN, can produce an indentation of the end of the atomically sharp tips inside the crystal while scanning. This observation is valid for the two types of tips involved in the simulation. In both cases the distortion or the disruption during scanning depended on how fast the displaced surface ions were able to return to their lattice sites with respect to the scanning speed. If the tip has already destroys the contacted sample as it scans, there will be no longer possible a repeating periodic structure on successive line scans.

5.2.2 1D pattern induced by an AFM tip on KBr

Scratches were produced and imaged using our home-built force microscope in UHV at room temperature. We used commercially available silicon cantilevers (section 2.2) with normal and torsional spring constants of about c_n=0.09 N/m and c_t=49 N/m. The radius of curvature of the tips was nominally below 15 nm. The same cantilevers were used for both scratching and imaging the modified areas. Two different KBr(001) surfaces were studied. Sample 1 was cleaved in situ, while sample 2 was cleaved in air and immediately transferred into the UHV chamber. Both samples were heated to 120 °C for 15 minutes. The different cleavage procedure affected the morphology of the surface significantly; on the sample cleaved in UHV atomically flat areas not wider than 100 nm were observed, whereas the surfaces cleaved in air revealed flat terraces larger than 1 μm. However, atomically clean surfaces are obtained by both methods [122].

Figure 5.2a shows the topography image of a groove on the surface of KBr(100), recorded after scratching the surface 512 times with a normal load F_N=26.6 nN and a scan velocity v=2.67 mm/s. The groove is surrounded by a pattern of 34 mounds aligned along the two sides, and by two mounds piled up at its ends. The topography at the ground of the groove appears modulated as well. The height difference between the top of the mounds and the bottom of the pits in the groove is about 2.5 nm. The distance between two adjacent pits or mounds is about 40 nm, as well as the distance between the two rows of mounds.

Figure 5.2b compares a cross section of the topography along the ground of the groove with a measurement of the lateral force recorded while scratching the groove. The topographic image has been recorded with very low load on the tip after the scratching experiment was finished. The topographical information

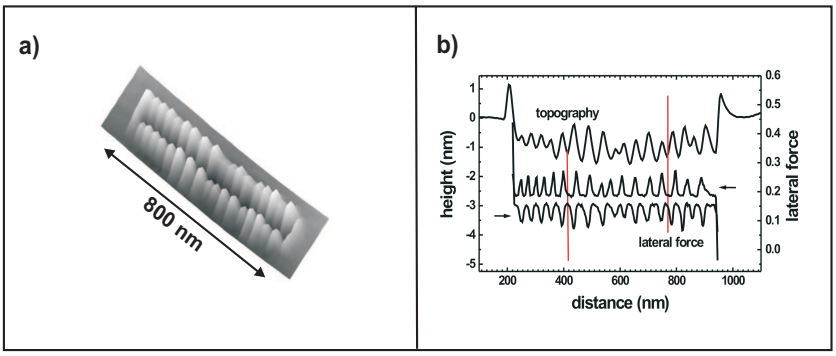

Figure 5.2: a) Topography image of a groove formed on KBr(001) after 512 scratches along the (100) direction with F_N=26.6 nN and v=2.67 mm/s (sample 1). b) Cross section of the topography along the ground of the groove and lateral force acquired while scratching the groove. The lower and upper parts of the lateral force loop were obtained while scanning forwards and backwards, as indicated by the arrows. The dotted lines indicate positions in the pits where the tip is decelerated as derived from an increase of the lateral force in either direction.

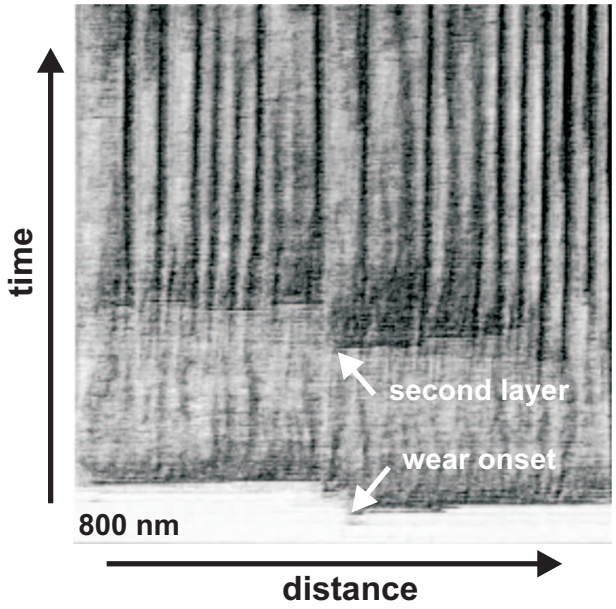

Figure 5.3: Development of lateral force with time while scratching a single line of 800 nm length forwards and backwards. In horizontal direction the lateral force during forward scan is plotted, where darker color means stronger lateral force; the vertical direction is the time axis.

recorded simultaneously with the scratching can not be used for the comparison due to strong cross talk between lateral and normal force at the high load required for scratching. The lateral force is modulated with the same periodicity as the topography along the groove. Note that there is no stick-slip characteristic but a continuous sliding with modulated lateral force, i.e., with modulated velocity in the tip. Any increase of the lateral force is a direct indication for a slower tip movement with respect to the movement of the support. Comparing topography and lateral force in fig. 5.2b we find that the lateral force starts to increase whenever the tip is at the edge of a pit between two mounds. The tip movement is decelerated at the slope of the mounds, and a lateral strain is built up. At a certain level the lateral force is high enough to pull the tip out of the pit and with some accelerated velocity the tip moves onto and over the mound. These results indicate that the formation of the regular ripples is related to an interplay between the developing topography and the lateral strain produced by the tip of the force microscope.

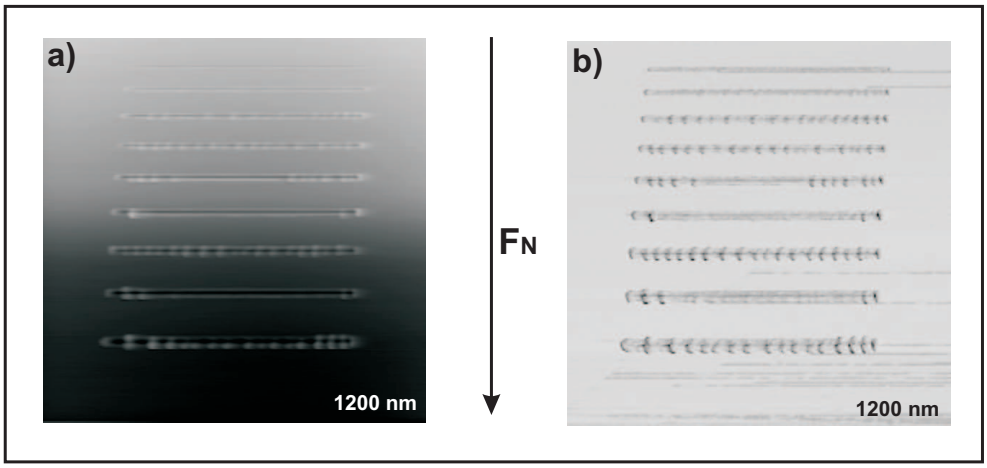

Figure 5.4: a) Topography and b) lateral force maps of a region scratched with the following loads (up to down): 1.7, 5.3, 8.8, 12.4, 15.9, 19.5, 23, 26.6, 30.1 μN. Frame size: 1.2 μm.

Figure 5.4 shows a series of grooves with a length of 800 nm produced by scratching the same surface 512 times with a velocity of 2.67 mm/s and with varying loads. There is a clear monotonous increase of the depth of the grooves and the height of the mounds piled up around the grooves with increasing load. However, the dependence of the development of undulated structures on the load is much less evident. Some grooves exhibit hardly any ripples at their edges, and some only close to their ends. There is no clear tendency in the effectiveness of ripple formation depending on the applied load. However, in numerous experiments we found that such ripples form for all loads and velocities after prolonged

scratching. To summarize these observations, we find that wear always increases with load, while the ripple formation is a more irregular process which, however, after some time always starts.

In order to visualize the onset of ripple formation, fig. 5.3 shows the lateral force recorded while scratching along one line as a function of time. For the first few scan lines, the friction force is low and no structure can be recognized. Wear starts then at a point in the center of the scan line, and spreads out first to the right and then to the left. The higher friction is caused by the enhanced interaction of the tip sliding in the groove compared to sliding on an atomically smooth terrace. The friction force is developing some faint structure, which is again lost in the course of further scanning. After about one third of the time represented in this figure, another instability similar to the one starting the whole process in the beginning is observed. Taking into account the depth of the final groove of about 0.6 nm (cf. fig. 5.2), it is plausible to assume that wear of a second atomic layer starts at that point. Now the ripple pattern in the lateral force evolves and is stable throughout the experiment. Unfortunately, we cannot quantify lateral force and topography at the same time. In order to avoid any disturbance of the lateral force measurement [123] by the distance feedback, the latter is extremely slow and maintains only a mean constant normal load.

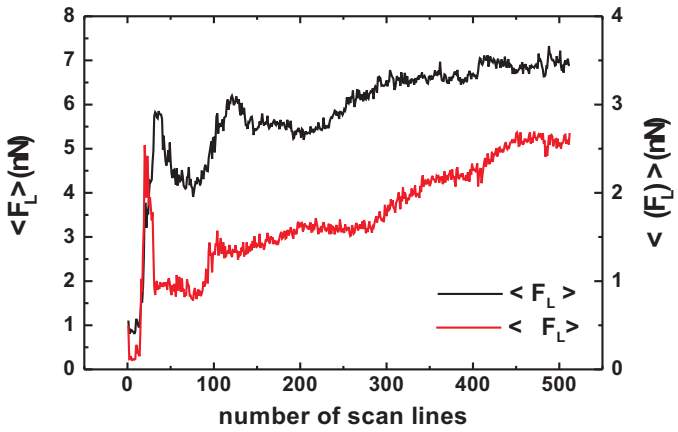

Figure 5.5: The development of the mean lateral force $<F_L>$ and of its standard deviation $<\delta F_L>$ while producing the ripple pattern shown in fig. 5.3.

It is worth mentioning that the lateral force is relatively strong and irregular each time after a new atomic layer starts to wear off. This is documented in the corresponding graph in fig. 5.5. The mean lateral force $<F_L>$ shows steplike increases, with a strong peak at the position of the first step and a less pronounced

peak at the position of the second. For longer scratching we have found that the mean lateral force slowly levels off. The standard deviation of the lateral force $<\delta F_L>$ exhibits steplike increases where a new atomic layer is eroded, reflecting the growing amplitude of the lateral force when the worn-off atoms are reorganized in form of the ripples. Judging from this graph, we might even identify the erosion of a third layer around the 280th and of a fourth layer around the 400th scan line. In repeated longer experiments we have not observed a saturation of the increase of the ripple amplitude. Again, the onset of erosion of the first two atomic layers is indicated by sharp peaks which reflect the irregularity of the atomic reorganization process.

5.2.3 Periodicity given by tip "shape"?

The distances between the tip-induced ripples on KBr increase slightly with an increase of the applied normal load.

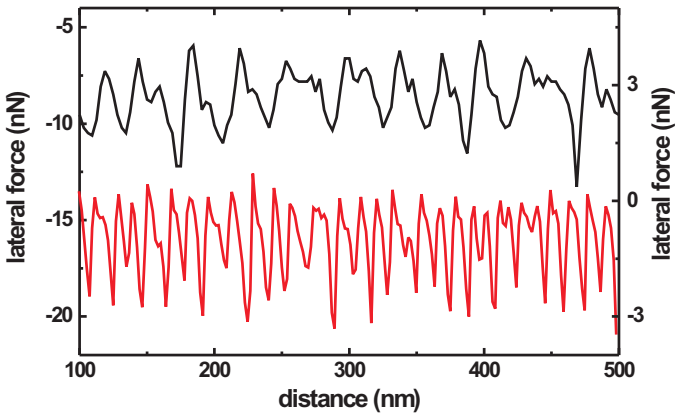

Figure 5.6: Lateral force recorded during the 1250th scratch using two different tips and samples (black curve is quantified by the left scale, red curve by the right one). The normal load (3.6 nN) was the same for both curves.

However, they vary significantly between experiments using different tips. Lateral force curves of the stable ripple pattern obtained in two different series of experiments are compiled in fig. 5.6. While the typical features described above are reproduced for all tips and samples, the ripple distances vary from 20 nm to 50 nm. This length scale matches the typical radii of force microscope tips. Therefore, we speculate that the distance between the ripples is correlated with the actual tip shape. It was observed a slightly increase of the ripple distance with load, which suggests that the increasing contact area as well influences the

ripple distance. In fig. 5.6 the curve with larger ripple distance shows higher values of the lateral force, indicating again a larger contact radius.

5.2.4 2D pattern induced by an AFM tip

Two-dimensional patterns in the lateral force with similar periodicity are obtained if the tip is scanning a square, by slowly moving along the (010) direction while scanning forwards and backwards along the (100) direction. Figure 5.7 shows the result of scanning 34 times a square frame of 300×300 nm^2, composed of 256 horizontal lines. The vertical distance between two consecutive scan lines is much smaller than the typical width of the grooves observed in fig. 5.4. A pattern of ripples is revealed, with a preferential alignment perpendicular to the fast scanning direction of the tip. Note that in the first frame the surface is flat and it does not presents holes, steps or any other structure. The typical wavelength of the ripples is about 40 nm.

On the surface cleaved in UHV (sample 2) the initial stages of the ripple formation were influenced by the cleavage steps (fig. 5.8). The steps are eroded and aligned perpendicular to the fast scanning direction, and serve as nucleation sites for the first ripples. After prolonged scanning, however, the pattern becomes independent of the original morphology and adopts a shape comparable to fig. 5.4.

5.2.5 Analogies

In a recent paper Friedrich et al. investigated the action of a localized moving disturbance which deposits or removes material from a surface [124]. They assumed that the surface profile evolves according to a generalized Kuramoto- Sivashinsky equation, which takes into account the inhomogeneity of the disturbance.

$$\frac{\partial h}{\partial t} = f(\mathbf{r}) \left[\frac{1}{1+(\nabla h)^2} + \nu \triangle^2 h + k \triangle^4 h \right] - v \frac{\partial h}{\partial x}, \tag{5.1}$$

The competition between a negative surface tension ν, which tends to increase the area of the surface, and a positive coefficient k, which accounts for the surface diffusion, leads to a periodic structuring of the surface with wavelength $\lambda \sim \sqrt{k/\nu}$. Similar mechanisms have been previously recognized as responsible for the ripple formation observed under ion sputtering [125], although in such a case the perturbation is not localized, but acts on the whole surface at the same time. In our case the negative surface tension can be identified with the stronger erosion in the pits connected with the higher strain exerted by the trapped tip. On the other hand, the perfect recrystallization of the piled-up mounds indicates that diffusion also plays a smoothing role for the ripple formation on KBr. It is interesting to note that thin films of KBr produced by molecular evaporation grow in form of pyramidal mounds, where the topmost terraces have typical sizes

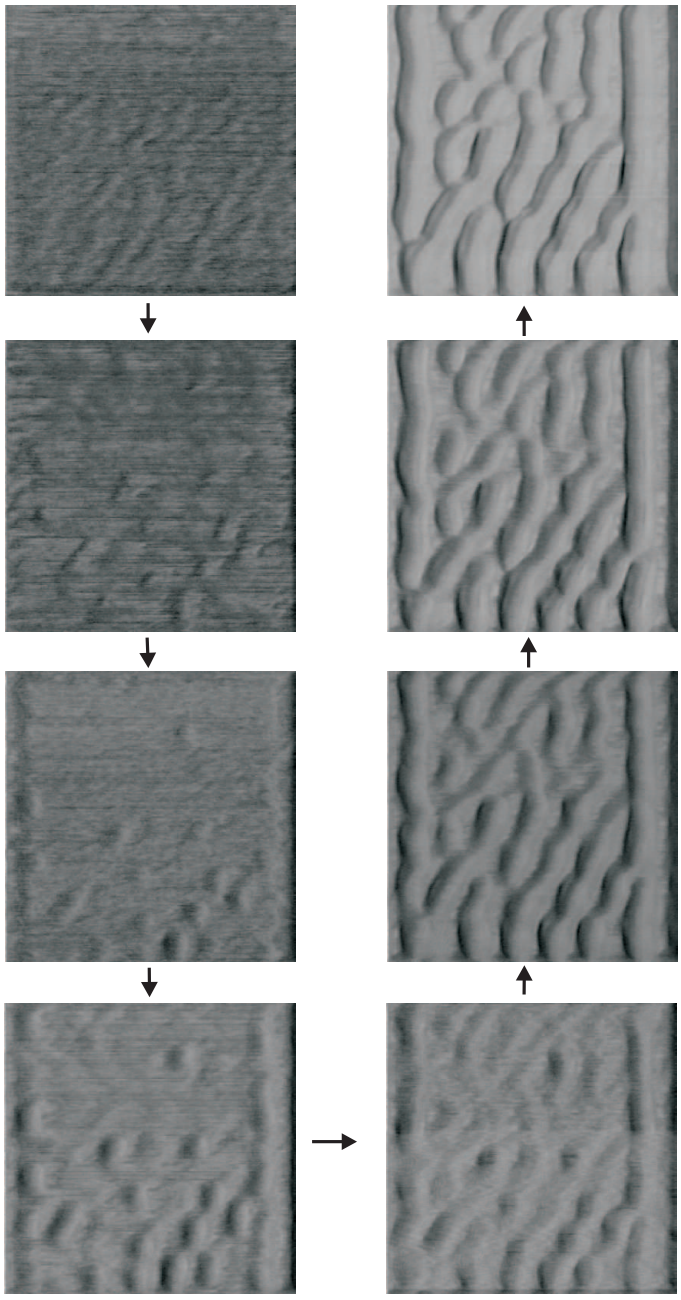

Figure 5.7: Lateral force images of square area scanned 35 times with higher load. The presented friction maps are obtained after 1st, 5th, 10th, 15th, 20th, 25th, 30th and respectively 35th complete scan over the same area. The eroded square has a side length of 500 nm.

in the range of 20-50 nm [126], in exactly the same size range we find for the ripple distances. In the present results, the relation between height and width of

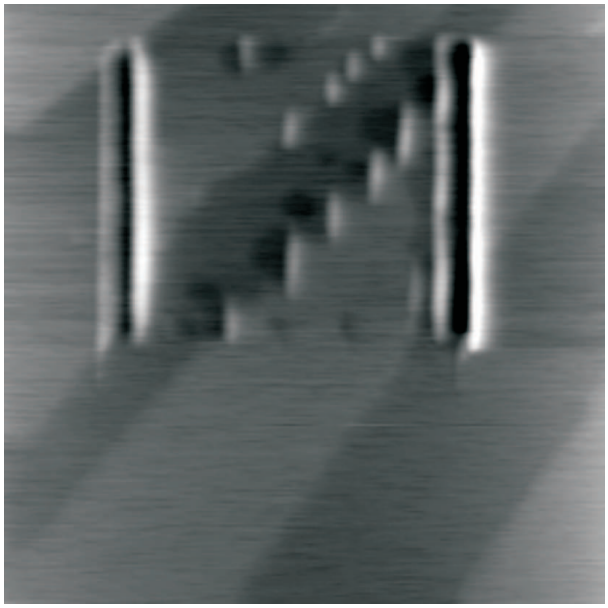

Figure 5.8: Topography images of a square area scanned before with higher load. Zoom out on KBr surface with cleavage steps running from the lower left to the upper right corner of the frame (sample 2). The eroded square has a side length of 500 nm.

the mounds is low compared to typical growth pyramids and, therefore, diffusion does not limit the further increase of the surface corrugation. This is reflected in the lack of saturation of the lateral force variation in fig. 5.3. Based on the experimental results, we cannot determinate the dominant parameter for the distance of the ripples. The weak dependence of the distance on the normal load may suggest that both a characteristic diffusion length and the shape of the tip might be important for the size of the developing structures.

5.3 Discussion

In the following, we will discuss the tip-induced process of ripple formation along the results presented in the previous sections. First of all, this process starts only after the onset of abrasive wear. No signs of topographic modulation have been observed without an erosion of at least one monolayer of KBr, i.e., without transfer of material. Elastic instabilities or plastic deformation related to creation or movement of dislocations can be excluded, when the strain energy produced by the scratching tip is smaller than the energy required for the creation of dislocations. Based on our observations, we believe that this is the case in our experiments. Similar arguments have been brought forward in the discussion

of nanoscale indentation of metals [127, 128]. Once an atomic layer is damaged at some specific spot, the whole layer is removed and its material reorganized in a process accompanied by strong, irregular friction. After some tens of scan lines (compare fig. 5.5) a more ordered structure is formed. This process was described in detail in a previous study [58] where it was shown that the material is continuously detached in small amounts of ion couples or small clusters. The debris at the end of the scratch, i.e., in front of the moving tip, perfectly recrystallizes in atomically flat terrace which exhibits exact atomic registry with the underlying substrate lattice. Some understanding of the process can be obtained from comparing the corrugated topography and lateral force profiles in fig. 5.2. The ripples probably emerge when material transported in front of the tip increases the friction, slowing down the tip movement until the lateral force is strong enough to make the tip jump over the mound of material. During following scan lines, existing mounds will collect further material and grow. In this scenario the minimal distance between two ripples would be given by the size of the tip, in agreement with the experimental findings.

5.3.1 Ripples on different surfaces and environments

In order to understand the influence of the environment on the process of ripples formation we performed the same experiment in air conditions. Scratches were produced and imaged using a commercial NI Nanoscope IV microscope operated in non-controlled environment. A new KBr(001) sample, cleaved in air, was studied. Under prolonged scanning, much longer than in UHV conditions, a pattern of ripple oriented perpendicular to the scan direction was revealed. It is important to mention that much higher loads are required in order to get a well developed structure on the surface. The high humidity conditions present during the experiment led to rather unstable undulated structure. The debris produced by the action of the tip had a large mobility, favored by the water layer present at the tip-sample interface. Fig. 5.9 presents the dependence on normal load of the periodicity of the developed structured in different situation, in UHV and air. Both dependence shows a rather linear increase of the wavelength with the load. In UHV, in the applied range of forces, the periodicity is slightly enhanced under the action of F_N. In air, bigger loads were applied leading to increased tip-surface contact areas, and therefore larger distances between the mounds or the pits of the ripples.

The phenomenon of ripple formation in friction force microscopy experiments on the nanometer scale occurs on a variety of surfaces. In the literature polymer surfaces seem to be privileged materials developing such structure [60]. Metal surfaces may also develop regular topographic features. In fig. 5.10a a similar result is presented, which has been obtained on an Al(111) surface in ultra high vacuum. Again, a two-dimensional pattern of ripples evolved under the scanning tip. The periodicity is of the same order of magnitude as for KBr, around 40-

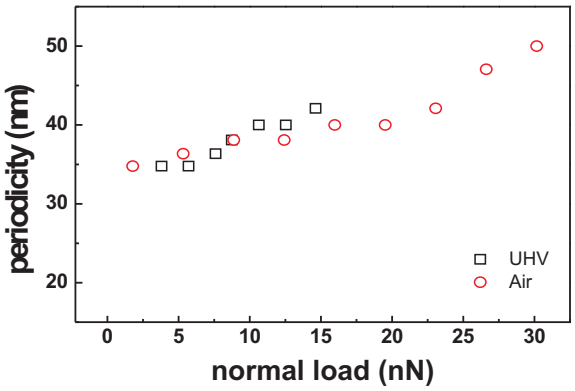

Figure 5.9: The periodicity of the ripples as function of the normal load. The back dots corresponds to the measurements performed in UHV, and the red ones to those performed in air.

50 nm. However, this surface is very sticky, and even at lowest normal load all topography images show significant disturbance by sticking effects. In contrast to KBr, the ripple pattern on Al(111) is unstable under prolonged scanning and turns into an irregular structure related to very strong wear processes. Fig. 5.10b shows the results of prolonged scanning over 1×1 μm rubber surface. Measurements performed by means of a commercial AFM (Nanoscope IV) under ambient conditions [129].
Again, a pattern of ripples is revealed, with a preferential alignment perpendicular to the fast scanning direction of the tip. For rubber the ripple structure got formed under prolonged scanning, after more than 20 repetitions, as in the case of KBr in air. The normal force necessary to initiate this process in air is ten or hundred times bigger. The typical wavelength of the ripples is about 160-200 nm.

The ripples formation is not restricted to a specific category of surfaces. The restructuring of the surface under the perturbing factor, in our case the AFM tip, can be obtained on a large variety materials and under controlled or uncontrolled environments. Probably, the periodicity is given by the size of the tip and depends slightly on the pressure applied by this on the scanned sample.

5.4 Conclusion

In conclusion, a detailed experimental report on the formation of regular topographic structures on a KBr surface upon scanning a force microscopy tip in

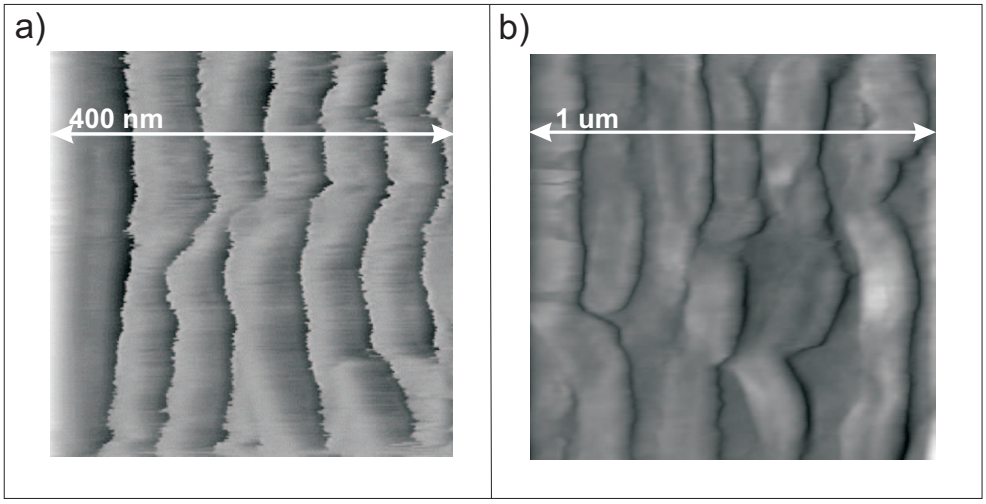

Figure 5.10: a) Al(111) surface with an eroded area of 400×400 nm^2 side length. Surface prepared and scratched under UHV conditions. b)Ripple formation on 1×1 μm rubber surface. Measurements were performed by means of a commercial AFM (*NanoscopeIV*) under ambient conditions.

contact with the sample is presented. Following abrasive wear of single atomic layers, the debris is moved and reorganized in an interplay between friction-induced strain and erosion, transport of material by the action of the tip, and possibly diffusion. The self-amplification of the evolving structures has an important impact on the tribological behavior, where stick-slip phenomena on different length scales are a general observation.

One can think of further applications of the ripple process formation. Under clean environments and corresponding normal loads, using tips with a desirable geometry, controlled surface developments can be obtained. Scanning one line or a square, linear or 2D structure can be produced. Thus, a deeper understanding of this process is important for the development of nanopatterned devices, such as optical grids.

List of abbreviations

AFM	Atomic Force Microscope
FFM	Friction Force Microscope
FMM	Friction Modulation Microscope
a.u.	arbitrary unit
KBr	Potassium bromide
MD	Molecular Dynamics
NaCl	Sodium chloride
NEMS	Nanoelectromechanical systems
MEMS	Microelectromechanical systems
SEM	Scanning Electron Microscope
Si	Silicon
STM	Scanning Tunnelling Microscope
UHV	Ultra High Vacuum

List of Figures

Bibliography

[1] B.N.J. Persson. *Sliding Friction. Physical Principles and Applications*. Kluwer Academic Press, 2000.

[2] L. da Vinci. *Codex Atlanticus*. 1478-1518, Biblioteca Ambrosiana, Milan, Italy.

[3] L. da Vinci. *Codex Arundel*. 1478-1518, Brithish Museum, London, UK.

[4] G. Amontons. *Memoires de l'academie royale A*. 257, 1706.

[5] L. Euler. *Sur la diminuation de la resistance du frotemant*. Mem. Math. Phys., 1748.

[6] L. Euler. *De Curvis Elasticic*. Acta Acad. Pretropolitanae, 1778.

[7] G.A. Coulomb. *Theorie des machines simples, en ayant egard au frotemant de leurs parties, et a la roideur des cordages*. Mem. Math. Phys., 161, Paris 1785.

[8] F.P. Bowden and D. Tabor. The friction and lubrication of solids. *Oxford Univ. Press, Oxford*, 1950.

[9] F.P. Bowden and D. Tabor. The friction and lubrication of solids, part ii. *Oxford Univ. Press, Oxford*, 1964.

[10] J.F. Archard. Single contacts and multiple encounters. *J. Appl. Phys.*, 32:1420, 1961.

[11] J.A. Greenwood and J.B.P. Williamson. Contact of nominally flat surfaces. *Prod. R. Soc. Lond. A*, 295:300, 1966.

[12] D.J. Whitehouse and J.F. Archard. The propierties of random surfaces of significance in their contact. *Prod. R. Soc. Lond. A*, 316:97, 1970.

[13] C.M. Mate, G.M. McClelland, R. Erlandsson, and S. Chiang. Atomic-scale friction of a tungsten tip on a graphite surface. *Phys. Rev. Lett.*, 59:1942, 1987.

[14] Y. Golan, C. Drummond, J. Israelachvili, and R. Tenne. In situ imaging of shearing contacts in the surface forces apparatus. *Wear*, 245:190, 2000.

[15] J. Krim and A. Widom. Damping of a crystal oscillator by an adsorbed monolayer and its relation to interfacial viscosity. *Phys. Rev. B*, 38:12184, 1988.

[16] H. Hertz. *J. Reine Angew. Math.*, 92:156, 1881.

[17] K.L. Johnson K. Kendal and A.D. Roberts. Surface energy and the contact of elastic solids. *Proc. R. Soc. Lond. A*, 324:301, 1971.

[18] K.L. Johnson. *Contact Mechanics*. Cambridge University Press, United Kingdom 1985.

[19] R.S. Bradley. *Phil. Mag.*, 13:853, 1992.

[20] B.V. Derjaguin, V.M. Muller, and Y.P. Toporov. Effect of contact deformations on adhesion of particles. *J. Coll. and Interface Sci.*, 67:378, 1975.

[21] C.A.J. Putman, M. Igarshi, and R: Kaneko. Single-asperity friction in friction force microscopy: The composite-tip model. *Appl. Phys. Lett.*, 66:3221, 1995.

[22] U.D. Schwarz, W. Allers, G. Gensterblum, and R. Wiesendanger. Low load friction behavior of epitaxial C60 monolayers under hertzian contact. *Phys. Rev. B*, 52:14976, 1995.

[23] R.W. Carpick, N. Agraït, D.F. Ogletree, and M. Salmeron. Measurement of interfacial shear (friction) with an ultrahigh vacuum atomic force microscope. *J. Vac. Sci. Technol. B*, 14:1289, 1995.

[24] M. Enachescu, R.J.A. van den Oetelaar, R.W. Carpick, D.F. Ogletree, C.F.J. Flipse, and M. Salmeron. Atomic force microscopy study of an ideally hard contact: The diamond(111)/tungsten carbide interface. *Phys. Rev. Lett.*, 81:1877, 1998.

[25] M.A. Lantz, S.J. OShea, M.E. Welland, and K.L. Johnson. Atomic-force-microscope study of contact area and friction on NbSe2. *Phys. Rev. B*, 55:10776, 1997.

[26] S. Fujisawa, E. Kishi, Y. Sugawara, and S. Morita. Load dependence of sticking-domain distribution in two-dimensional atomic scale friction of NaF(100) surface. *Tribol. Lett.*, 1:21, 1995.

[27] S. Fujisawa, E. Kishi, Y. Sugawara, and S. Morita. Load dependence of two-dimensional atomic-scale friction. *Phys. Rev. B*, 52:5302, 1995.

[28] W. Zhong and D. Tománek. 1st principles of atomic-scale friction. *Phys. Rev. Lett.*, 64:3054, 1990.

[29] T. Gyalog, M. Bammerlin, R. Lüthi, E. Meyer, and H. Thomas. Mechanism of atomic friction. *Europhys. Lett.*, 31:269, 1995.

[30] N. Sasaki, K. Kobayashi, and M. Tsukada. Atomic-scale friction image of graphite in atomic-force microscopy. *Phys. Rev. B*, 54:2138, 1996.

[31] H. Holscher, U.D. Schwarz, and R. Wiesendanger. Modelling of the scan process in lateral force microscopy. *Surface Science*, 375:395, 1997.

[32] K.L. Johnson and J. Woodhouse. Stick-slip motion in the atomic force microscope. *Tribol. Lett.*, 5:155, 1998.

[33] J. Colchero, O. Marti, and J. Mlynek. *Forces in Scanning Probe Methods: Friction on an atomic scale.* Kluwer Academic, Dordrecht, 1995, p.345.

[34] G.A. Tomlinson. *Philos. Mag. Ser.*, 7:905, 1929.

[35] E. Gnecco, R. Bennewitz, T. Gyalog, and E. Meyer. Friction experiments on nanometer scale. *J. Phys.: Condens. Matter*, 13:619, 2001.

[36] D. Tománek, W. Zhong, and H. Thomas. Calculation of an atomically modulated friction force in atomic-force microscopy. *Europhys. Lett.*, 15:887, 1991.

[37] M. Hirano, K. Shinjo, R. Kaneko, and Y. Murata. Anisotropy of frictional forces in muscovite mica. *Phys. Rev. Lett.*, 67:2642, 1991.

[38] P.M. McGuiggan and J.N. Israelachvili. Adhesion and short-range forces between surfaces. effects of surface lattice mismatch. *J. Mater. Res.*, 5:2232, 1990.

[39] M. Hirano. Superlubricity: a state of vanishing friction. *Wear*, 254:932, 2003.

[40] K. Shinjo and M. Hirano. Surface structures and conductance at initial stages in epitaxy of metals on a Si(111) surface. *Surface Science*, 283:473, 1993.

[41] M.S. Sørensen, K.W. Jakobsen, and P. Stoltze. Simulations of atomic-scale sliding friction. *Phys. Rev. B*, 53:2101, 1996.

[42] M. Hirano, K. Shinjo, R. Kaneko, and Y. Murata. Observation of superlubricity by scanning tunneling microscopy. *Phys. Rev. Lett.*, 78:1448, 1997.

[43] J.M. Martin, C. Donnet, Th. Le Mogne, and Th. Epicier. Superlubricity of molybdenum disulphide. *Phys. Rev. B*, 48:10583, 1993.

[44] M. Dienwiebel, G.S. Verhoeven, N. Pradeep, J.W.M. Frenken, J.A. Heimberg, and H.W. Zandbergen. Superlubricity on graphite. *Phys. Rev. Lett.*, 126101:92, 2004.

[45] T. Zijlstra, J.A. Heimber, E. van der Drift, D. Glastra van Loon, M. Dienwiebel, L.E.M. de Groot, and J.W.M. Frenken. Fabrication of a novel scanning probe device for quantitative nanotribology. *Sensors and Actuators A: Physical*, 84:18, 2000.

[46] H. Bluhm, U.D. Schwarz, and R. Wiesendanger. Origin of the ferroelectric domain contrast observed in lateral force microscopy. *Phys. Rev. B*, 57:161, 1998.

[47] R.M. Overney, H.Takano, M. Fujihira, W. Paulus, and H. Ringsdorf. Anisotropy in friction and molecular stick-slip motion. *Phys. Rev. Lett.*, 72:3546, 1994.

[48] H. Takano and M. Fujihira. Study of molecular scale friction on stearic acid crystals by friction force microscopy. *J. Vac. Sci. Technol. B*, 14:1272, 1996.

[49] D. Gourdon, N.A. Burnham, A. Kulik, E. Dupas, F. Oulevey, G. Gremaud, D. Stamou, M. Liley, Z. Dienes, H. Vogel, and C. Duschl. The dependence of friction anisotropies on themolecular organisation of LB films as observed by AFM. *Tribol. Lett.*, 3:317, 1997.

[50] M. Liley, D. Gourdon, D. Stamou, U. Meseth, T.M. Fischer, C. Lautz, H. Stahlberg, H. Vogel, N.A. Burnham, and C. Duschl. Friction anisotropy and asymmetry of a compliant monolayer induced by a small molecular tilt. *Science*, 280:273, 1998.

[51] M.H. Müser. Structural lubricity: Role of dimension and symmetry. *Europhys. Lett.*, 97:66, 2004.

[52] L. Wenning and M.H. Müser. Friction laws for elastic nanoscale contacts. *Europhys. Lett.*, 54:693, 2004.

[53] M.H. Müser and M.O. Robbins. *Atomic Computer Simulation of Friction between Solids*. Proceeding for Simu Conference "Challeges in Molecular Simulation", 2002, p.101-117.

[54] J.P. Gao, W.D. Luedtke, and U. Landman. Friction control in thin films lubrication. *J. Phys. Chem. B.*, 107:5033, 1998.

[55] A. Cochard, L. Bureau, and T. Baumberger. Stabilisation of frictional sliding by normal load modulation. *Trans. ASME*, 70:220, 2003.

[56] M. Heuberger, C. Drummond, and J. Israelachvili. Coupling of normal and transverse motions during frictional sliding. *J. Phys. Chem. B*, 102:5038, 1998.

[57] R. Lüthi, E. Meyer, M. Bammerlin, L. Howald, H. Haefke, T. Lehmann, Ch. Loppacher, and H.-J. Güntherodt. Friction on the atomic scale: An ultrahigh vacuum atomic force microscopy study on ionic crystals. *J. Vac. Sci. Technol. B*, 14:1280, 1996.

[58] E. Gnecco, R. Bennewitz, and E. Meyer. Abrasive wear on the atomic scale. *Phys. Rev. Lett.*, 88:215501, 2002.

[59] S. Kopta and M. Salmeron. The atomic scale origin of wear on mica and its contribution to friction. 113:8249, 2000.

[60] O.M. Leung and M.C. Goh. Orientational ordering of polymers by atomic force microscope tip-surface interection. *Science*, 255:64, 1992.

[61] Z. Elkaakour, J. Aimé nad T. Bouhacina, C. Odin, and T. Masuda. Bundle formation of polymers with an atomic force microscope in contract mode: A friction versus peeling process. *Phys. Rev. Lett.*, 73:3231, 1994.

[62] R.A. Bagnold. *The Physics of Blown Sand and Desert Dunes*. Mathuen, London, 1941.

[63] A. Schallamach. How does rubber slide? *Wear*, 17:301, 1972.

[64] U. Valbusa, C. Boragno, and F. Buatier de Mongeot. Nanostructuring surfaces by ion sputtering. *J. Phys.: Condens. Matter*, 14:8153, 2002.

[65] M. Andersson, A. Iline, F. Stietz, and F. Träger. Formation of gold nanowires through self-assembly during scanning force microscopy. *Appl. Phys. A*, 68:609, 1999.

[66] A.I. Livshits and A.L. Shluger. Self-lubrication in scanning-force-microscope image formation on ionic surfaces. *Phys. Rev. B*, 56:12482, 1997.

[67] A. Buldum and C. Ciraci. Contact, nanoindentation, and sliding friction. *Phys. Rev. B*, 57:2468, 1998.

[68] R. Komanduri, N. Chandrasakaran, and L.M. Raff. Molecular dynamics simulation of atomic-scale friction. *Phys. Rev. B*, 61:14007, 2000.

[69] J. Li, K.J. Van Vliet, T. Zhu, S. Yip, and S. Suresh. Atomistic mechanisms governing elastic limit and incipient plasticity in crystals. *Nature*, 418:307, 2002.

[70] R.M. Overney, R. Lüthi, H. Haefke, J. Frommer, E. Meyer, H.-J. Güntherodt, S. Hild, and J. Fuhrmann. An atomic force microscopy study of corona-treated polypropylene films. *Appl. Surf. Sci.*, 64:197, 1993.

[71] R. Lüthi, H. Haefke, E. Meyer, L. Howald, H.P. Lang, G. Gerth, and H.-J. Güntherodt. Frictional and atomic-scale study of c60 thin films by scanning force microscopy. *Z. Phys. B. Condensed Matter*, 95:1, 1994.

[72] E. Meyer, R. Overney, D. Brodbeck, L. Howald, R. Lüthi, J. Frommer, and H.-J. Güntherodt. Friction and wear of langmuir-blodgett films observed by friction force microscopy. *Phys. Rev. Lett.*, 69:1777, 1992.

[73] R. Bennewitz, T. Gyalog, M. Guggisberg, M. Bammerlin, E. Meyer, and H.-J. Güntherodt. Atomic-scale stick-slip processes on Cu(111). *Phys. Rev. B*, 60:11301, 1999.

[74] G. Binning, Ch. Gerber, E. Stoll, T.R. Albrecht, and C.F. Quate. Atomic resolution with atomic force microscopy. *Europhys. Lett.*, 3:1281, 1987.

[75] T.R. Albrecht and C.F. Quate. Atomic resolution imaging of a nonconductor by atomic force microscopy. *J. Appl. Phys.*, 62:2599, 1987.

[76] E. Meyer, H. Heinzelmann, H. Rudin, and H.-J. Güntherodt. Atomic resolution on LiF(001) by atomic force microscopy. *Z. Phys. B. Condensed Matter*, 79:3, 1990.

[77] E. Meyer, H.-J. Güntherodt, H. Haefke, G. Gerth, and M. Krohn. Atomic resolution on the AgBr(001) surface by atomic force microscopy. *Europhys. Lett.*, 15:319, 1991.

[78] Nanosensors: http://www. nanosensors.com.

[79] M. Dienwiebel, N. Pradeep, G.S. Verhoeven, H.W. Zandbergen, and J.W.M. Frenken. Model experiments of superlubricity of graphite. *Surface Science*, 576:197, 2005.

[80] G.M. McClelland. *Friction at Weakly Interacting Interfaces.* Springer-Verlag, Berlin, 1990, p. 1.

[81] G.M. McClelland and J.N. Glosli. *Fundamentals of Friction.* Spinger-Verlag, 1992, p. 405.

[82] J.S. Helman and W. Baltensperger. Nonmonotonic velocity dependence of atomic friction. *Phys. Rev. B*, 49:3831, 1994.

[83] C. Fusco and A. Fasolino. Velocity dependence of atomic-scale friction: A comparative study of the one- and two-dimensional tomlinson model. *Phys. Rev. B*, 71:045413, 2005.

[84] Y. Hoshi, T. Kawagishi, and H. Kawakatzu. Velocity dependence and limitations of friction force microscopy of mica and graphite. *Jpn. J. App. Phys.- Part 1*, 39:3804, 2000.

[85] L. Howald, E. Meyer, R. Lüthi, H. Haefke, R. Overney, H. Rudin, and H.-J. Güntherodt. Multifunctional probe microscope for facile operation in ultrahigh vacuum. *Appl. Phys. Lett.*, 63:117, 1993.

[86] R.W. Carpick, Q. Dai, D.F. Ogletree, and M. Salmeron. Friction force microscopy investigations of potassium halide surfaces in ultrahigh vacuum: structure, friction and surface modification. *Tribol. Lett.*, 5:91, 1998.

[87] E. Gnecco, R. Bennewitz, T. Gyalog an d Ch. Loppacher, M. Bammerlin, E. Meyer, and H.-J. Güntherodt. Velocity dependence of atomic friction. *Phys. Rev. Lett.*, 84:1172, 2000.

[88] R. Lüthi, E. Meyer, H. Haefke, L. Howald, W. Gutmannbauer, M. Guggisberg, M. Bammerlin, and H.-J. Güntherodt. Nanotribology: an UHV-SFM study on thin films of C60 and AgBr. *Surface Science*, 338:247, 1995.

[89] L. Howald, R. Lüthi, E. Meyer, G. Gerth, H. Haefke, R. Overney, and H.-J. Güntherodt. Friction force microscopy on clean surfaces of NaCl, NaF, and AgBr. *J. Vac. Sci. Technol. B*, 12:2227, 1994.

[90] E. Meyer, H. Hug, and R. Bennewitz. *Scanning Probe Microscopy*. Springer-Verlag, Berlin, 2003.

[91] E. Riedo, E. Gnecco, R. Bennewitz, E. Meyer, and H. Brune. Interaction potential and hopping dynamics governing sliding friction. *Phys. Rev. Lett.*, 91:084502, 2003.

[92] R. Carpick, D.F. Ogletree, and M. Salmeron. Lateral stiffness: A new nanomechanical measurement for the determination of shear strengths with friction force microscopy. *Appl. Phys. Lett.*, 70:1548, 1997.

[93] L. Bartels, G. Meyer, and K.-H. Rieder. Basic steps of lateral manipuation of single atoms and diatomic clusters with a scanning tunneling microscope tip. *Phys. Rev. Lett.*, 79:697, 1997.

[94] L.N. Kantorovich and T. Trevethan. General theory of microscopic dynamical response in surface probe microscopy: From imaging to dissipation. *Phys. Rev. Lett.*, 93:236102, 2004.

[95] P. Reimann and M. Evstigneev. Nonmonotonic velocity dependence of atomic friction. *Phys. Rev. Lett.*, 93:230802, 2004.

[96] N.S. Tambe and B. Bhushan. Scale dependence of micro/nano-friction and adhesion of MEMS/NEMS materials, coatings and lubricants. *Nanotechnology*, 15:1561, 2004.

[97] A.N. Cleland and M.L. Roukes. A nanometre-scale mechanical electrometer. *Nature*, 392:160, 1998.

[98] J. Kerssemarkers and J.Th.M. De Hosson. Probing the interface potential in stick/slip friction by a lateral force modulation technique. *Surface Science*, 417:281, 1998.

[99] P. Maivald, H.J. Butt, S.A.C. Gould, C.B. Prater, B. Dreke, J.A. Gurley, V.B. Elings, and P.K. Hansma. Using force modulation to image surface elasticities with the atomic force microscope. *Nanotechnology*, 2:103, 1991.

[100] O. Kolosov and K. Yamanaka. Coupling of normal and transverse motions during frictional sliding. *Jpn. J. Appl. Phys.- Part 2*, 32:L1095, 1993.

[101] T. Sakamoto, M. Abo, and S. Kakunai. Friction reduction in a stick-slip process under vibratory load. friction change with low-frequency load. *Journal of Japanese Society of Tribologists*, page 36, 1991.

[102] A.A. Polycarpou and A. Soom. Boundary and mixed friction in the presence of dynamic normal loads: Part I - System model. *J. Tribol.*, 117:255, 1995.

[103] U. Rabe, K. Janser, and W. Arnold. Vibrations of free and surface-coupled atomic force microscope cantilevers: Theory and experiment. *Rev. Sci. Instr.*, 67:3281, 1996.

[104] G. Behme and T. Hesjedal. Influence of surface acoustic waves on lateral forces in scanning force microscopies. *J. Appl. Phys.*, 89:4850, 2001.

[105] W.F. Stokey. *Shock and Vibration Handbook*. C.M. Harris and C.E. Crede, McGraw-Hill , New York, 1976, pp.7-1ff.

[106] T. Drobek, R.W. Stark, and W.M. Heckl. Determination of shear stiffness based on thermal noise analysis in atomic force microscopy: Passive overtone microscopy. *Phys. Rev. B*, 64:045401, 2001.

[107] K. Miura, N. Sasaki, and S. Kamiya. Friction mechanisms of graphite from a single-atomic tip to a large-area flake tip. *Phys. Rev. B*, 69:075420, 2004.

[108] A. Socoliuc, R. Bennewitz, E. Gnecco, and E. Meyer. Transition from stick-slip to continuous sliding in atomic friction: Entering a new regime of ultra-low friction. *Phys. Rev. Lett.*, 92:134301, 2004.

[109] J.M.R. Weaver and D.W. Abraham. High resolution atomic force microscopy potentiometry. *J. Vac. Sci. Technol. B*, 92:1559, 1991.

[110] S. Belaidi, P. Girard, and G. Leveque. Electrostatic forces acting on the tip in atomic force microscopy: Modelization and comparison with analytic expressions. *J. Appl. Phys.*, 81:1023, 1997.

[111] M.G. Rozman, M. Urbakh, and J. Klafter. Controlling chaotic friction. *Phys. Rev. E*, 57:7340, 1998.

[112] Th. Schimmel, K.Friemelt, J. Küppers, M.Ch. Lux-Steiner, H.-J. Güntherodt, D. Anselmetti, and E. Meyer. Forces in scanning probe methods. *NATO ASI-Series, Kluwer, Dordrecht*, 525, 1995.

[113] F. Dinelli, S.K. Biswas, G.A.D. Briggs, and O.V. Kolosov. Ultrasound induced lubricity in microscopic contact. *Appl. Phys. Lett.*, 71:1177, 1997.

[114] L. Bureau, T. Baumberger, and C. Caroli. Shear response of a frictional interface to a normal load modulation. *Phys. Rev. E*, 62:6810, 2000.

[115] B. Bhushan and V.N. Koinkar. Tribological studies of silicon for magnetic recording applications. *J. Appl. Phys.*, 75:5741, 1994.

[116] X. Jin and W.N. Unertl. Submicrometer modification of polymer surfaces with a surface force microscope. *Appl. Phys. Lett.*, 61:657, 1992.

[117] Y. Kim, J.L. Huang, and C.M. Lieber. Characterization of nanometer scale wear and oxidation of transition metal dichalcogenide lubricants by atomic force microscopy. *Appl. Phys. Lett.*, 59:3404, 1991.

[118] R. Bennewitz, E. Genecco, T. Gyalog, and E. Meyer. Atomic friction studies on well-defined surfaces. *Tribol. Lett.*, 10:51, 2001.

[119] A.L. Shluger, A.L. Rohl, R.T. Williams, and R.M. Wilson. Model of scanning force microscopy on ionic surfaces. *Phys. Rev. B*, 52:11398, 1995.

[120] W.D. Luedtke and U. Landman. Solid and liquid junctions. *Comp. Mater. Sci.*, 1:1, 1992.

[121] O. Tomagnini, F. Ercolessi, and E. Tosatti. Microscopic interaction between a gold tip and a Pb(110) surface. *Surface Science*, 287:1041, 1993.

[122] R. Bennewitz, A.S. Foster, L.N. Kantorovich, M. Bammerlin, Ch. Loppacher, S. Schär, M. Guggisberg, E. Meyer, H.-J. Güntherodt, and A.L. Shluger. Atomically resolved steps and kinks on nacl islands on cu(111): Experiment and theory. *Phys. Rev. B*, 62:2074, 2000.

[123] U.D. Schwarz, P. Köster, and R. Wiesendanger. Quantitative analysis of lateral force microscopy experiments. *Rev. Sci. Instr.*, 67:2560, 1996.

[124] R. Friederich, G. Randons, T. Ditzinger, and A. Henning. Ripple formation through an interface instability from moving growth and erosion source. *Phys. Rev. Lett.*, 85:4884, 2000.

[125] R. Cuerno, H. Makse, S. Tomassone, H. Harrington, and H. Stanley. Stochastic model for surface erosion via ion sputtering: Dynamical evolution from ripple morphology to rough morphology. *Phys. Rev. Lett.*, 75:4464, 1995.

[126] J. Kaolodziej, B. Such, P. Czuba, F. Krok, P. Piatkowski, and M. Szymonski. Scanning-tunneling/atomic-force microscopy study of the growth of KBr films on InSb(001). *Surface Science*, 506:12, 2002.

[127] J. Belak and I.F. Stowers. *Fundamentals of Friction.* Kluwer Academic Press, Dordrecht, 1992, p. 511.

[128] U. Dürig. *Physics of Sliding Friction.* Kluwer Academic Publishers, Dordrecht, 1996, p. 299.

[129] Veeco Metrology Group: http://www.di.com.

List of publications

Publications

- Atomic-scale control of friction by actuation of nanometer-sized contacts. A. Socoliuc, E. Gnecco, S. Maier, O. Pfeiffer, A. Baratoff, R. Bennewitz and E. Meyer. *submitted to Science*.

- Transition from Stick-Slip to Continuous Sliding in Atomic Friction: Entering a New Regime of Ultralow Friction. A. Socoliuc, R. Bennewitz, E. Gnecco and E. Meyer. *Phys. Rev. Lett.* 92: 134131, 2004.

- related articles:
  1)Reducing Friction without Oil. Highlighted by *Physical Review Focus*, April 2004.
  2) Ultra-Low Friction, Without Lubricants. Highlighted by *Physics News Update*, 677, 18 March 2004.
  3)Nanoscale friction slides downwards. Highlighted by *Nanotechweb*, 1 April 2004.
  4) Frictionless sliding on the atomic scale. E. Gnecco, A. Socoliuc and E. Meyer, *Imaging and Microscopy*, June 2004.
  5) Slippery Nanoworld. E. Gnecco, A. Socoliuc, E. Meyer, A. Baratoff, R. Bennewitz, M. Dienwiebel, J. Frenken. *Europhysicsnews*, January-February 2005.

- Ripple formation induced by localized abrasion. A. Socoliuc, E. Gnecco, R. Bennewitz and E. Meyer *Phys. Rev. B*, 68: 115416, 2003.

- Friction and wear on the atomic scale. E. Gnecco, R. Bennewitz, A. Socoliuc and E. Meyer. *Wear* 254: 859, 2003.

- Atomic friction and wear. R. Bennewitz, E. Gnecco, A. Socoliuc, U. Wyder and E. Meyer *Abstract of Papers of the American Chemical Society* 227: U812-U813 060-COLL Part 1, MAR 28 2004.

- Friction and wear on the atomic scale. E. Gnecco, R. Bennewitz, O. Pfeiffer, A. Socoliuc and E. Meyer. *Springer Handbook of Nanotechnology*, Springer-Verlag, Heidelberg, Germany, 2004.

Talks

- Nanowear: From atomic abrasion to ripple. A. Socoliuc, E. Gnecco, R. Bennewitz, E. Meyer. *2nd ESF-Nanotribology Workshop*, 20-23 October 2003, Antalya, Turkey.

- Towards minimum energy dissipated in atomic friction. Transition from dissipative friction to a new regime of ultra-low friction. A. Socoliuc, E. Gnecco, R. Bennewitz, E. Meyer. *2004 Swiss Physical Society (EPS) Meeting*, 3-4 March 2004, Neuchatel, Switzerland.

- Towards minimum energy dissipated in atomic friction. Transition from dissipative friction to a new regime of ultra-low friction. A. Socoliuc, E. Gnecco, R. Bennewitz, E. Meyer. *IUVSTA*, 28 June - 2 July 2004, Venice, Italy.

Acknowledgements

I am grateful to my supervisor Prof. Dr. Ernst Meyer for giving me the opportunity to work in his group. He accepted my application for PH.D. in his group in a difficult moment for me. I want to thank for his help and trust during the last years. I would like to thank Prof. Dr. Güntherodt for the opportunity and financial support to work for a project within the NCCR program.

I want to express my sincere gratitude to Prof. Roland Bennewitz and Dr. Enrico Gnecco for their indispensable and direct supervising. I learned (I hope I did!) how important is to be able to express clearly a point of view, but mainly the advantage of asking straight questions. I am grateful to all of them for the fruitful work in the lab and the discussions we've experienced.

I would like to thank to Prof. Dr. Alexis Baratoff for his theoretical support, his effort of helping me with his impressive and large knowledge.

I would like to thank to all former and actual members of Ernst Meyer's group: Laurent Nony, Adrian Wetzel, Oliver Pfieffer, Dominique Schär, Sacha Schär, Sabine Maier, Lars Zimmerli for the nice time we spent in the lab (but not only) and for the excellent collaboration we had. Laurent has been for me a very good example of pure perfectionism and of never giving up. I've always been happy to receive his advices. Adrian was the person I spent a lot of time in the lab with, trying to implement tuning forks as force sensors in AFM. This was one of the nicest periods in the lab. I want thus to thank to him for the amazing large knowledge and for his effort of sharing them with me. Dominique helped me with Scanita, the new scanning software he developed. I want to thank to Oli for his permanent support in the lab, to Sabine, Lars, Sacha and for the good collaboration.

I would like to thank to all the people in the house (Jean Pierre, Wilfried, Iris, Peter, Javad...and many others) for the friendly atmosphere, for the discussions during lunch time and coffee (or cigarette) brakes.

I would like to thank G. Weaver, A. Fischer, A. Kalt, B. Kammermann and J. Vetter from the secretaries for the administrative work.

This work was financially supported from the National Centers of Competence in Research (NCCR).

Special thanks to Julien for his support, patient and sometimes constructive criticism. Thanks!

As vrea sa multumesc Prof. Dr. Gh. Singurel pentru incredere, sfaturi si ajutorul dumnealui la inceputul doctoratului meu. Toate cunostiintele insusite acolo, la Universitatea de Fizica din Iasi, la catedra de Optica si Spectroscopie, dar nu numai, mi-au fost de un real ajutor in acesti aproape patru ani de doctorat.

Sincera mea apreciere as vrea sa o adresez lui Dr. Dorinel Verdes care mi-a fost mereu un exemplu de studiu si seriozitate. Fara ajutorul si sfaturile lui poate ca nu as fi ajuns, astazi, cu succes, la finalul acestui doctorat. Multe, multe multumiri!

Multe multumiri parintilor mei si surorii mele, ei au fost tot timpul un factor incurajator in viata mea.

Basel, Switzerland — Anisoara Socoliuc
18th May 2005

Curriculum Vitae

Anisoara Socoliuc

2.08.1975	born in Focsani, Romania
1982 - 1986	Primary School, Focsani, Romania
1986 - 1990	Secondary School, Focsani, Romania
1990 - 1994	High School "Al.I. Cuza", Focsani, Romania
1994 - 1999	Faculty of Physics,'Al.I. Cuza' University, Iasi, Romania
June 1999	Diploma in Physics: *Nuclear Magnetic Resonance - treated by density matrix formalism*
1999 - 2001	Master Studies in "Optics and Spectroscopy"
Jan-Oct 2000	exchange student within Socrates program, Solid State Department, University of Gent, Belgium
Feb 2001	Master thesis: *Target voltage changes during DC reactive sputtering of silver in argon/nitrogen plasma*
Nov. 2001 - June 2005	Doctoral studies in the group of Prof. Dr. Ernst Meyer at the Institute of Physics, University of Basel

I would like to thank to the following persons for their influence on my professional formation:

G. Apostol, E. Poll, Gh. Singurel, D. Verdes, E. Meyer, R. Bennewitz, A. Baratoff, E. Gnecco.